Multimode rotationally symmetric bosonic codes from group-theoretic construction

Multimode rotationally symmetric bosonic codes from group-theoretic construction

Rabsan Galib Ahmed,[1,2,3] Adithi Udupa,[2] and Giulia Ferrini[2,*]

[1]*Department of Physical Sciences, Indian Institute of Science Education and Research Mohali, Punjab 140306, India*

[2]*Wallenberg Centre for Quantum Technology, Department of Microtechnology and Nanoscience, Department of Microtechnology and Nanoscience, Chalmers University of Technology, Göteborg SE-412 96, Sweden*

[3]*Institute for Quantum Computing, University of Waterloo and Department of Applied Mathematics, University of Waterloo, Waterloo, Canada*

(Received 28 October 2025; accepted 6 May 2026; published 21 May 2026)

We introduce a family of multimode, rotationally symmetric bosonic codes inspired by the group-theoretic framework introduced by Denys and Leverrier [Phys. Rev. Lett. **133**, 240603 (2024)]. Such a construction inverts the traditional paradigm of code design by identifying codes from the requirement that a group of chosen logical gates should be implemented by means of physically simple logical operations, such as linear optics. Leveraging previously unexplored degrees of freedom within this framework, our construction results in codes that display rotational symmetry across multiple modes, while enabling linear-optics implementation of the full Pauli group. These codes exhibit improved protection against dephasing noise, outperforming both single-mode analogues and earlier multimode constructions. Notably, they allow exact correction of correlated dephasing and support qudit encoding in arbitrary dimensions. We analytically construct and numerically benchmark two-mode binomial code instances, and demonstrate that, unlike single-mode rotationally symmetric bosonic codes, these exhibit no trade-off between protection against dephasing and photon loss.

DOI: 10.1103/xt48-fxt5

I. INTRODUCTION

Bosonic codes encode a logical qubit into the infinite-dimensional Hilbert space of a quantum harmonic oscillator, enabling protection of quantum information by tailoring the encoding to dominant physical noise processes such as photon loss and dephasing [1]. In contrast to conventional qubit-based encodings, which typically require a large number of physical qubits to correct generic errors, bosonic codes can exploit the structure and bias of noise at the hardware level, thereby achieving error suppression with significantly reduced overhead. Recent experiments have demonstrated a prolongation of logical lifetimes beyond those of the underlying physical components, reaching the so-called breakeven regime [2,3]. Furthermore, concatenating bosonic codes with higher-level quantum error-correcting codes can substantially reduce the resource requirements of fault-tolerant architectures [4–11]. This in turns induces an increased algorithmic performance as compared to the use of standard qubits [12]. However, despite these advantages, important challenges remain, including construction of codes that can tackle a wide range of noise errors and construction of gates that are easily implementable in the existing hardware. Addressing these limitations is essential for assessing the true potential of bosonic codes in scalable fault-tolerant quantum computing.

One way to understand the performance of bosonic codes is in terms of their symmetries. For instance, N-order rotationally symmetric bosonic (RSB) codes [13] have a specific structure of the code words in Fock space, where only Fock states with multiples of N are allowed. This structure implies that RSB codes allow for detecting the loss or gain of up to $N-1$ photons at the same time, while also tolerating phase errors of magnitude up to π/N. While such codes have the potential to break even in relevant parameter regimes, finding bosonic codes with better performance is essential to further reduce the overhead of physical qubits needed in practical implementations of concatenated codes. Furthermore, the implementation of relevant gates such as the logical X gate on such codes is complicated and requires the use of auxiliary qubits. In particular, for single-mode rotation-symmetric codes, such operations generally require carefully optimized control pulses [13]. Therefore, it is essential to design bosonic codes with good quantum error-correcting (QEC) properties, and at the same time with easily implementable sets of logical gates.

While usual approaches to the design of QEC codes consist of first introducing a code, and then finding the operations that implement the logical gates on that code, Ref. [14] takes an opposite approach. It provides a group-theoretic construction where one first selects a chosen group of logical gates, e.g., the Pauli group, to be implemented by simple physical operations, e.g., linear optics, and then a corresponding code is identified, where the desired logical gates are implemented by means of the chosen simple physical operations. However, the construction in Ref. [14] did not take into account general symmetries of the code and their connection to QEC properties.

In this work, we exploit some previously unexplored freedom in the construction of Ref. [14], to allow for a more general construction yielding a family of multimode bosonic codes with rotational symmetry, which we therefore call

*Contact author: ferrini@chalmers.se

multimode RSB codes. These codes retain the advantage of the ones in Ref. [14], as their logical Pauli operations remain implementable via linear optics, while also offering enhanced performance against dephasing errors compared with the corresponding instances in Ref. [14]. Furthermore, this multimode extension also allows us to encode qudits of arbitrary dimension. We perform a detailed analytical analysis of this family of codes for the qubit case, and also provide numerical results of the performance for a specific instance, namely, the dual-rail binomial code, which can be thought as the two-mode generalization of the binomial code [13,15]. We provide analytical and numerical evidence showing that, in contrast to the single-mode version of this code, which displays a trade-off between the capability of detecting loss or dephasing errors at increasing order of the discrete rotational symmetry N [13], the dual-rail binomial code offers a simultaneous improvement of the error detection capability, yielding an overall improvement in the error correction performance over the single-mode case. Furthermore, we show that any two-mode RSB code in our family of codes offers perfect protection against correlated dephasing.

II. PRELIMINARIES

The essential idea behind the group-theoretic encoding of Ref. [14] is to find a subspace of the Hilbert space of a given physical system, called the *codespace*, that is isomorphic to the logical space, such that a group of logical operations are *easily implementable*. It takes as inputs: a group, G, and its representations, Λ and Π, on the logical and physical Hilbert spaces, respectively, where Π is constructed using a set of physical operations that we define as easily implementable. The output of this construction is a family of codespaces, from which the codespace performing optimally against relevant noise channels can be chosen. As an application, a two-mode bosonic code has been proposed in Ref. [14], when G is chosen to be isomorphic to the Pauli group, $\langle X, Z\rangle$, and the physical representation, Π, is constructed with passive linear operations on two modes. The resulting *Pauli code* has been shown to perform better than the dual-rail code against the pure loss channel in the two modes. However, the construction itself offers more freedom in choosing G and Π than it was explored in Ref. [14].

III. MULTIMODE ROTATION-SYMMETRIC BOSONIC CODES

We start by showing that an extended construction allows us for encoding a qudit, having a d-dimensional Hilbert space, in a family of multimode RSB codes, hosted by d bosonic modes. The Pauli group for a qudit is generated by X and Z. In the computational basis, their actions are given by $X|k\rangle = |k \oplus 1\rangle$, $Z|k\rangle = \omega_d^k |k\rangle$, where $\omega_d = e^{2\pi i/d}$. Inspired by, but distinctly from, the construction of Ref. [14], we choose the group G to be $G = \langle g, h | h^{2N} = e\rangle$ for an *even* N and the representations $\lambda(g) = X$, $\lambda(h) = Z$ and [16]

$$\pi(g) = \hat{U}_{\rm BS}\left(\prod_{i=1}^{d-1} e^{-i\frac{\pi}{2}\hat{G}^-_{i,i+1}}\right)^{\dagger}\hat{U}_{\rm BS}^{\dagger}, \tag{1}$$

$$\pi(h) = \hat{U}_{\rm BS} e^{i\frac{2\pi}{Nd}\hat{a}_1^{\dagger}\hat{a}_1}\hat{U}_{\rm BS}^{\dagger}. \tag{2}$$

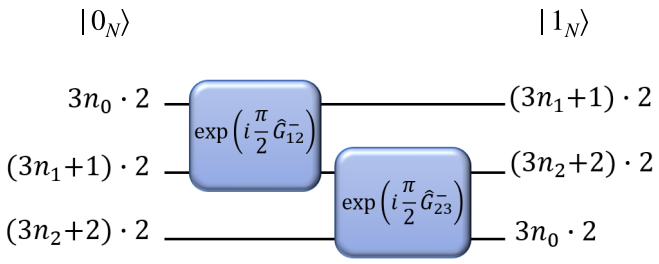

FIG. 1. Application of the logical X gate on a qutrit ($d = 3$) encoded in a three-mode rotation-symmetric bosonic code of order $N = 2$. Each of the lines indicates a single bosonic mode.

Here, $\hat{U}_{\rm BS} := \exp\{i\sum_{j,k=1;j<k}^{d}(\theta^-_{jk}\hat{G}^-_{jk} + \theta^+_{jk}\hat{G}^+_{jk})\}$ is a general passive linear operation generated by beam splitters on all pairs of modes (j,k), with $\hat{G}^+_{jk} = \hat{a}_j^{\dagger}\hat{a}_k + \hat{a}_k^{\dagger}\hat{a}_j$ and $\hat{G}^-_{jk} = i(\hat{a}_j^{\dagger}\hat{a}_k - \hat{a}_k^{\dagger}\hat{a}_j)$ and $\theta^{\pm}$'s some real numbers parametrizing $\hat{U}_{\rm BS}$. Crucially, this mode mixing operation, absent in the construction of Ref. [14], endows the code with additional freedom in the choice of the encoding modes, which, as we will see, will result in an enhancement of the code performance. A beam splitter for encoding a multimode bosonic code was considered with NOON states in Ref. [17]. We find that the d-dimensional subspace of d physical modes, where Eqs. (1) and (2) operate as logical X and Z, respectively, is spanned by the computational code words

$$|k_N\rangle = \hat{U}_{\rm BS}\sum_{\{n_i\}=0}^{\infty} f_{n_0\cdots n_{d-1}}\bigotimes_{j=k}^{k\oplus(d-1)}|(dn_j + j)N\rangle, \tag{3}$$

where $\oplus$ is addition modulo d, the indexes $\{n_i\}$ run between 0 and ∞, and $f_{n_0\cdots n_{d-1}}$'s are coefficients that can be choosen freely, provided they satisfy normalization. The derivation is given in Appendix A. We also assume that if the upper limit on the product sign, $\bigotimes$, is less than the lower limit, then the index j runs a period through $\mathbb{Z}/d\mathbb{Z}$. For example, when $k = 1$, $d = 3$, j runs through 1, 2, 0; hence, the product state is $|(3n_1 + 1)N\rangle \otimes |(3n_2 + 2)N\rangle \otimes |3n_0 N\rangle$. In each of the modes, we have an order-N rotation symmetry, as can be verified by applying the order-N rotation symmetry operator $\hat{R}_N^{(k)} = e^{i2\pi\hat{n}_k/N}$ to the code word, where $\hat{n}_k = \hat{U}_{\rm BS}\hat{a}_k^{\dagger}\hat{a}_k\hat{U}_{\rm BS}^{\dagger}$. As an illustration, the action of the logical operator X stemming from Eq. (1) on a qutrit ($d = 3$) encoded in a three-mode rotation-symmetric bosonic code of order $N = 2$ is illustrated in Fig. 1. Note the similarity of the Fock-space structure with the case of single-mode RSB qudits, as defined in Appendix F of Ref. [18]. Distinct multimode bosonic codes with rotational symmetry were introduced from homological rotor codes in Ref. [19]. Other codes exhibiting rotational symmetry have been studied in the context of single-photon implementations of GKP states [20].

IV. TWO-MODE INSTANCE AND KNILL-LAFLAMME CONDITIONS

As a special case of the multimode encoding of a qudit, we focus on the case when $d = 2$: encoding a qubit in two

bosonic modes. The most general code words are explicitly given by

$$|0_N\rangle = \hat{U}_{\rm BS} \sum_{m,n} f_{mn} |2mN, (2n+1)N\rangle, \tag{4}$$

$$|1_N\rangle = \hat{U}_{\rm BS} \sum_{m,n} f_{mn} |(2n+1)N, 2mN\rangle, \tag{5}$$

with $\hat{U}_{\rm BS} = \exp[i\delta(\hat{G}^{+}_{12}\sin\phi + \hat{G}^{-}_{12}\cos\phi)]$.

By construction, the logical bit-flip gate X acting on these code words is implemented as $\hat{U}_{\rm BS} e^{-i\pi \hat{G}^{-}_{12}/2} \hat{U}^{\dagger}_{\rm BS}$, which corresponds to a swap operation. The logical phase-flip gate Z is implemented by $\hat{U}_{\rm BS} e^{i\pi \hat{a}_1^{\dagger}\hat{a}_1/N} \hat{U}^{\dagger}_{\rm BS}$ [21]. We focus on loss and dephasing channels. In the general case of the combined channel of the two, the Kraus representation is given by

$$\mathcal{N}_L \circ \mathcal{N}_D \sim \left\{ \hat{L}^{(1)}_p \hat{L}^{(2)}_q \hat{D}^{(1)}_r \hat{D}^{(2)}_s : p, q, r, s \in \mathbb{N}_0 \right\}, \tag{6}$$

where the Kraus operators for the loss and dephasing channel in each mode, $i = 1, 2$, are, respectively, given by

$$\hat{L}^{(i)}_p = \sqrt{\frac{(1-e^{-\kappa_i t})^p}{p!}} e^{-\frac{1}{2}\kappa_i t\, \hat{a}_i^{\dagger}\hat{a}_i}\, \hat{a}_i^p, \tag{7}$$

$$\hat{D}^{(i)}_r = \sqrt{\frac{(\gamma_i t)^r}{r!}} e^{-\frac{1}{2}\gamma_i t\, (\hat{a}_i^{\dagger}\hat{a}_i)^2} (\hat{a}_i^{\dagger}\hat{a}_i)^r. \tag{8}$$

The loss and dephasing strength of the channels are, respectively, quantified by the parameters $\kappa_i t$ and $\gamma_i t$ in each mode. The evolution of the encoded state up to first order under this combined channel is provided in Appendix A.

We then study the Knill-Laflamme (KL) conditions for the above codes for arbitrary coefficients f_{mn} for individual channels. For a purely loss channel, up to first order in the noise strength, we show in Appendix B 1 that the KL conditions are satisfied provided the coefficients obey $\sum_{m,n} |f_{mn}|^2 (m-n) = \frac{1}{2}$. For a purely dephasing channel, up to first order in the dephasing noise strength, we see that the KL conditions depend on the encoding angles of the beam splitter. The KL conditions upto first order in $\gamma_i t$ are satisfied for $N \geqslant 4$ when $\delta = \pi/4$ (Appendix C 1).

For both these noise models, in order to correct the effect of the noise channel up to the first order in the noise strength for an arbitrary logical state prepared in the code words [Eqs. (4) and (5)], we propose a two-mode extension of the recovery map outlined for the simplest single-mode bosonic codes [2,15]: A modular number measurement (a generalized number-parity measurement) indicates the errorsyndrome and corresponding unitary operators are applied. The details of the analytical recovery map for the case of loss and dephasing are provided, respectively, in Appendixes B 2 and C 2.

V. COMPARISON WITH OTHER CODES

We now turn to which families of codes are subsumed in our code family. If we disregard the beam splitter $\hat{U}_{\rm BS}$, choosing $f_{mn} \propto \frac{e^{-2|\alpha|^2}}{\sqrt{(2mN)!((2n+1)N)!}} \alpha^{2mN} \alpha^{(2n+1)N}$ yields the concatenation of a cat code with a dual-rail code [22], distinct from the cat repetition code [23]. This code is also distinct from the pair cat codes found in Ref. [24], where the code words are eigenstate of the difference between the number operators of the two modes. The choice $f_{mn} = 1\ \forall m, n$ yields instead the concatenated dual-rail ideal number-phase code [13], distinct from the repetition number-phase code. For numerical analysis of the performance of our codes, we choose the instance $f_{mn} = \frac{1}{\sqrt{2}}$ when $(m, n) = (0, 0)$ and $(1, 0)$, and $f_{mn} = 0$ for any other (m, n). This yields the family of dual-rail binomial code (DRBC) for $K = 2$,

$$|0_N\rangle = \hat{U}_{\rm BS}(\delta, \phi) \frac{1}{\sqrt{2}} (|0\rangle + |2N\rangle) \otimes |N\rangle, \tag{9}$$

$$|1_N\rangle = \hat{U}_{\rm BS}(\delta, \phi) |N\rangle \otimes \frac{1}{\sqrt{2}} (|0\rangle + |2N\rangle), \tag{10}$$

with N the order of rotation symmetry, and where the encoding-dependent angles (δ, ϕ), here explicited, parametrize the beam-splitting operator $\hat{U}_{\rm BS}$. These code words are similar, although distinct, to the two-qubit binomial encoded Bell state of Ref. [25] and the two-mode codes of Refs. [26,27]. As compared to concatenation with repetition code, the relatively uniform distribution of the bosonic excitations across the two modes of our codes holds potential for increased QEC performance.

VI. NUMERICAL RESULTS FOR DRBC UNDER LOSSES AND DEPHASING CHANNELS

We now analyze the performance of the DRBC with $K = 2$ defined in Eqs. (9) and (10), for various values of the beam-splitter parameter. We compare to the "breakeven threshold," which is defined here as the average fidelity of a logical qubit constructed with the ground state ($|0\rangle$) and the first excited state ($|1\rangle$) of a harmonic oscillator, called the *trivial encoding*, subjected to relevant noise channels but without a recovery operation [2,3]. We also compare the performance of our codes with the single-mode binomial code, as well as with the two-mode Chuang-Leung-Yamamoto (CLY) code of Ref. [28]. Note that the CLY is generally not an instantiation of the family of codes proposed here.

In Fig. 2(a), we analyze the performance under a pure dephasing channel. We find with both numerical and analytical analyses (as we will detail further) that the optimal performance of the DRBC with $K = 2$ against Gaussian dephasing noise is achieved for the choice of the beam-splitter angles $\delta = \pi/4,\ 3\pi/4, \phi = \pi/(2N)$. The condition $\delta = \pi/4,\ 3\pi/4$ also corroborates the optimal encoding angles that we found through the KL conditions. For this choice of angles, we see that the performance of the DRBC with $K = 2$ is significantly better than for the case of the single-mode binomial code. In Fig. 2(b), we study the performance under pure loss channel, and we see that the DRBC behaves very similar to the single-mode case while still doing better than CLY code.

For single-mode RSB codes, there is a trade-off [13]: While the performance against losses increases at increasing N (up to an optimal value of N), for dephasing it decreases at increasing N. After this optimal value of N, the performance decreases with N for both noise channels. Strikingly, we observe instead a significant improvement in performance under the dephasing noise channel of our DRBC with $K = 2$ for the optimal choice of the encoding angles (δ, ϕ), which results in a simultaneous improvement of the performance with increasing N up to an optimal value of N [see Figs. 2(a) and 2(b)]. In Fig. 2(c), we present the results for the combined

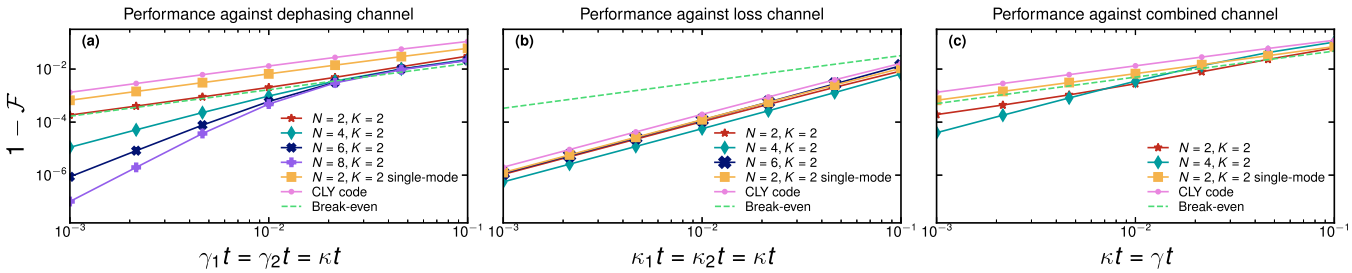

FIG. 2. Performance of the simple instances in Eqs. (9) and (10) of the two-mode rotation-symmetric code for the DRBC instances against (a) the dephasing channel with equal rates in both the modes, $\gamma_1 = \gamma_2 = \gamma$, (b) the loss channel with $\kappa_1 = \kappa_2 = \kappa$, and (c) a combination of both of these noisy channels with equal strengths in both the modes and with $\gamma = \kappa$. In all the three cases, we have chosen the optimal values of the beam-splitter angles (δ, ϕ) and we note that under the loss channel, the performance is independent of this choice. We also compare against the $N = 2$, $K = 2$ single-mode binomial code, the two-mode CLY code, and the breakeven. For dephasing, we also report the performance for $K = 2$, $N = 6$ and $K = 2$, $N = 8$, corroborating the performance increase at increasing N. We note that under the dephasing channel the evolution is restricted to a smaller subspace than the full Hilbert space that is required to describe a general evolution of the code words. This allows us to go to higher values of N to evaluate the performance of the code under the purely dephasing channel. We note that the optimum value of N under the loss channel displayed in panel (b) is around $N = 4$, which is similar to the corresponding case of the single-mode code [13]. Our two-mode codes show comparable performance to the corresponding N-order single-mode code under the loss channel, while they enhance the performance quite significantly against the dephasing channel [panel (a)].

dephasing-loss channel. The performance analysis for each of the noise models studied has been carried out by numerically solving the semidefinite programming (SDP) of finding the optimal recovery map [29]. Evaluating the performance for larger values of N and K using semidefinite programming becomes computationally challenging due to the rapidly increasing dimension of the Hilbert space. We provide numerical results on near-optimal fidelity that supports and extends the results obtained from SDP in Appendix D.

VII. UNDERSTANDING THE CODE PERFOMANCE AGAINST DEPHASING IN TERMS OF KNILL-LAFLAMME CONDITIONS AND CODE WORDS DISTINGUISHABILITY

For dephasing noise using the continuous Kraus representation, we show in Appendix E 1 that, for optimal angles $\delta = \pi/4, 3\pi/4$, $\phi = \pi/(2N)$, as N approaches infinity, the KL conditions for dual code words get closer to being exactly satisfied at any order of dephasing parameter. This validates the enhancement of performance at increasing N observed numerically. This increased performance as compared to the case of single-mode RSB codes can be further analyzed in terms of the code words' distinguishability under phase measurements. In a previous study [30], it was found that the performance of the single-mode rotation-symmetric codes for the Knill teleportation-based error-correcting (telecorrection) circuit against a purely dephasing noise is upper bounded by a monotically increasing function of the distinguishability between the dual code words, $|\pm_N\rangle$. In order to assess this distinguishability, one can employ the *canonical phase measurement* [13,31]. What was essentially found in Ref. [30] is that, as long as the probability distributions of the outcomes of the phase measurements for the code words, $|+_N\rangle$ and $|-_N\rangle$, do not significantly overlap under the evolution of a dephasing noise, it is possible to recover the logical state faithfully on average. Here, we extend this understanding to the case of two-mode rotation-symmetric codes by analyzing the phase measurements on the two modes. Unlike the case of single-mode codes, where the phase measurement outcomes lie in a circle, $[0, 2\pi) \cong S^1$, those in the case of two-mode codes lie in a torus, $S^1 \times S^1$. Therefore, in contrast to the single-mode codes where the distributions inevitably overlap in the circle, S^1, for the two-mode codes, with different choices of the encoding angles, δ, ϕ, the distributions can be made to avoid each other on the torus, $S^1 \times S^1$ (see Appendix E 2 for more details). We emphasize that, despite these arguments are based on distinguishability with respect to phase measurements, for correcting the dephasing noise to the leading orders for our two-mode code we use the modular number measurement to reveal the error syndrome as described in Appendixes B 2 and C 2.

We have also verified that the increase in performance of the DRBC for the optimal choice of the encoding angles, as compared to the single-mode binomial code, is robust even in the case of more sophisticated instances of dephasing channels, such as non-Markovian dephasing induced by random telegraph noise [30,32–36] (see Appendix F).

VIII. PERFORMANCE OF TWO-MODE RSB UNDER CORRELATED DEPHASING

Correlated dephasing can arise, e.g., as a result of the usually strong dephasing of flux tunable couplers such as SNAIL-based modes [37,38], noise that is picked up by the coupled bosonic modes. This can be modeled through a stochastic interaction Hamiltonian, $\hat{H}(t) = \nu c(t)(\hat{a}_1^\dagger \hat{a}_1 + \hat{a}_2^\dagger \hat{a}_2)$, where $c(t)$ is a stochastic variable. The effective noise channel is given in this case by

$$\mathcal{N}(\hat{\rho}) = \int_{-\infty}^{\infty} d\phi \; p_t(\phi) e^{i\phi(\hat{n}_1+\hat{n}_2)} \; \hat{\rho} \; e^{-i\phi(\hat{n}_1+\hat{n}_2)}. \tag{11}$$

Here, we show that for any choice of two-mode RSB code in Eqs. (4) and (5), the quantum circuit in Fig. 3 corrects exactly any such arbitrary correlated dephasing noise of the form in Eq. (11). Here, modes 1, 2 and 3, 4 encode the control

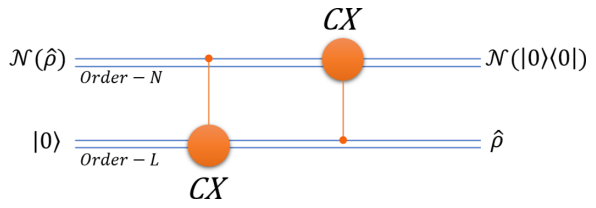

FIG. 3. Exact error-correcting circuit for correlated stochastic dephasing noise.

and the target qubits, respectively. The first controlled-X (CX) gate in Fig. 3 between two qubits encoded in order-N (control qubit) and order-M (target qubit) two-mode RSB code is implemented by the unitary $\mathrm{CX}NL = \exp(i\frac{\pi}{2N}\hat{n}_1 \otimes \hat{G}^{-}_{34})$. The second control unitary in Fig. 3 is given by $\exp(i\frac{\pi}{2N}\hat{n}_3 \otimes \hat{G}^{-}_{12})$. The two CX gates act as a swap gate, since the auxuliary mode is prepared in the logical state $|0\rangle$, and the correlated dephasing noise commutes through the CX gates, effectively swapping the noise-free state in the data rail to the auxiliary mode rail. In Appendix G, we provide a more detail derivation of the action of this circuit.

IX. APPLICATION OF OTHER GATES

The group of logical operators that we have chosen to be implemented through the *easy* operations, namely, the passive linear operations, is the Pauli group. However, that is not enough to achieve universal quantum compution. For that purpose, we additionally give a prescription for the application of the Hadamard gate (H), the phase gate (S), the T gate (T), and the two-qubit control-Z gate (CZ). Similarly to the case of the Pauli code discussed in Ref. [14], for our family of codes, for general even N, the S and the CZ gate can be applied using the nonlinear interactions of a microwave resonator [13]. Explicitly, for an even-N two-mode code, we have $\hat{S}_N = \exp(i\frac{\pi}{2N^2}\hat{n}_1^2)$, implementable using the self-Kerr interaction. The CZ gate between two qubits encoded in order N and order M can be applied similarly using the cross-Kerr interaction between two microwave resonator: $\mathrm{CZ}_{NM} = \exp(i\frac{\pi}{NM}\hat{n}_1 \otimes \hat{n}_3)$ [13], where the interaction happens between the first mode of each of the two encoded bosonic qubits. The H and T gates can be implemented using teleported gates, similar to what was proposed in Ref. [13]. For this purpose, an auxiliary qubit, encoded in two modes, is initially prepared in the states, $|+_N\rangle = \frac{1}{\sqrt{2}}(|0_N\rangle + |1_N\rangle)$ and $|T_N\rangle = \frac{1}{\sqrt{2}}(|0_N\rangle + e^{i\pi/4}|1_N\rangle)$, respectively, followed by a coupling to the two-mode data qubit using a CZ gate and a phase measurement on the data qubit. The resultant state of the auxiliary qubit contains the desired action of the gates up to an action of a logical X. The circuits are included in Appendix H.

X. CONCLUSIVE REMARKS AND OPEN QUESTIONS

We have introduced a family of multimode bosonic codes, which extends the rotationally symmetric bosonic codes introduced in Ref. [13] to the multimode, multidimensional case, by endowing the group theoretic construction introduced in Ref. [14] with the addition of beam splitters mixing the code words. An analysis of the two-mode dual-rail binomial instance for $K = 2$ reveals increased performance as compared to the single-mode case, in particular against dephasing noise, where the trade-off between resilience toward dephasing and loss errors at increasing discrete symmetry order N that affects the single-mode RSB codes (up to the optimum N) is resolved. This increase in performance achieved by increasing the number of modes in the codes echoes similar results found for translationally symmetric bosonic codes [39,40], but was not explored yet for RSB codes, to the best of our knowledge.

Several directions for further research arise from our work. For example, the very general code words presented in Eq. (3) yield a family of codes, with vast space for numerical optimization of the parameters, given a specific noise model, such as qudit dimensionality, order of rotational symmetry, and coefficients of the superposition. Furthermore, for the codes studied in this work we have chosen the Pauli group as the group to be implemented covariantly; it is an interesting question to ask what codes would stem by selecting other representations of the Clifford group or of groups homomorphically equivalent to it, than those considered in Ref. [14]. Finally, it is interesting to consider the case where physically implementable operations are not constrained to passive linear optical operations, but correspond instead to more sophisticated operations, such as those implementable with superconducting circuits [41,42].

ACKNOWLEDGMENTS

We acknowledge useful discussions with Tahereh Abad, Victor Albert, Axel Eriksson, Yvonne Gao, Simone Gasparinetti, Mats Granath, Trond Haug, Kunal Dhanraj Helambe, Maryam Khanahmadi, Martin Jirelow, Anthony Leverrier, Anja Metelmann, Lukas Splitthof, Peter van Loock, and Suocheng Zhao. We acknowledge Alberto Salvador for the numerical calculations on near-optimal fidelity results reported in the Appendix, as well as Julius Andersson, Carl Svensson, Hang Zhou, and Griffin Hiscoke for having derived the Knill-Laflamme conditions for the case of losses to second order in the loss rate. We thank Debjyoti Biswas and Nikhil Sharma for useful cross-validation of Knill-Laflamme conditions of loss channel. G.F. acknowledges funding from the European Union's Horizon Europe Framework Programme (EIC Pathfinder Challenge project Veriqub) under Grant Agreement No. 101114899, the Olle Engkvist Foundation, and the Swedish Research Council through the Project Grant VR DAIQUIRI. G.F. and A.U. acknowledge support from the Knut and Alice Wallenberg Foundation through the Wallenberg Center for Quantum Technology (WACQT). G.F., A.U., and R.G.A. acknowledge funding from Chalmers Area of Advance Nano, as well as resources at the Chalmers Centre for Computational Science and Engineering (C3SE).

DATA AVAILABILITY

The data that support the findings of this article are not publicly available. The data are available from the authors upon reasonable request.

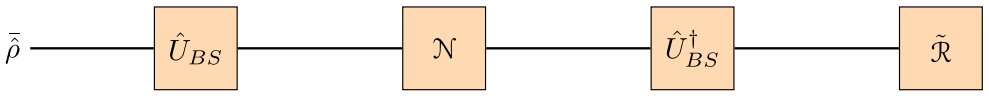

FIG. 4. An encoding and error-correcting procedure for the rotation-symmetric codes on two modes.

APPENDIX A: MULTIMODE ROTATION-SYMMETRIC CODE WORDS

In this Appendix, we provide a derivation of the qudit code words [Eq. (3)]. First, note that unlike Ref. [14], where both the group G and the physical representation Π are isomorphic to the Pauli group, we have utilized the fact that it is sufficient for there to exist a homomorphism, Λ, from G to the Pauli group and a physical representation, Π, that acts as Λ on at least one two-dimensional subspace.

For the derivation, it suffices to work out the case for $\hat{U}_{\rm BS} = \mathbb{I}$. We start by considering the general superposition of all possible states supported by d modes, given by

$$|k_N\rangle = \sum_{\{m_i\}=0}^{\infty} f^{(k)}_{m_0,\ldots,m_{d-1}} |m_0, m_1, \ldots, m_{d-1}\rangle. \tag{A1}$$

By imposing that the physical representation of the group element h acts as in Eq. (2), i.e., $\Pi(h)|k_N\rangle = e^{i\frac{2\pi}{Nd}\hat{a}_1^{\dagger}\hat{a}_1}|k_N\rangle = \omega_d^k|k_N\rangle$, with $\omega_d = e^{2\pi i/d}$, we find

$$f^{(k)}_{m_0,\ldots,m_{d-1}} = 0, \quad \text{unless } e^{i\frac{2\pi}{Nd}m_0} = e^{i\frac{2\pi k}{d}} \Rightarrow m_0 = (n_0 d + k)N, \forall n_0 \in \mathbb{N}_0. \tag{A2}$$

By imposing the physical representation of group element g, we require that $\Pi(g)|k_N\rangle = |(k \oplus 1)_N\rangle$. Using the relation $e^{i\frac{\pi}{2}\hat{G}^{-}_{i,i+1}}\hat{a}_i^{\dagger}e^{-i\frac{\pi}{2}\hat{G}^{-}_{i,i+1}} = -\hat{a}_{i+1}^{\dagger}$, we obtain

$$f^{(k)}_{m_0,\ldots,m_{d-1}}(-1)^{\sum_{i=1}^{d-1} m_i} = f^{(k\oplus 1)}_{m_1,\ldots,m_{d-1},m_0}. \tag{A3}$$

From Eq. (A2), we also see that $f^{(k\oplus 1)}_{m_1,\ldots,m_{d-1},m_0} = 0$, unless $m_1 = [n_1 d + (k \oplus 1)]N$. This implies

$$f^{(k)}_{m_0,\ldots,m_{d-1}} = 0, \quad \text{unless } m_1 = [n_1 d + (k \oplus 1)]N. \tag{A4}$$

Similarly, applying $\Pi(g)$ on $|k \oplus 1\rangle$, we arrive at the condition $f^{(k\oplus 1)}_{m_1,\ldots,m_0}(-1)^{\sum_{i=1}^{d-1} m_i} = f^{(k\oplus 2)}_{m_2,\ldots,m_0,m_1}$, where we again use Eq. (A2) to obtain the fact that $f^{(k\oplus 2)}_{m_2,\ldots,m_1}$, and thus $f^{(k)}_{m_0,\ldots,m_{d-1}}$ is equal to 0, unless $m_2 = [n_2 d + (k \oplus 2)]N$.

By induction, we therefore have

$$f^{(k)}_{m_0,\ldots,m_j,\ldots,m_{d-1}} = 0, \quad \text{unless } m_j = [n_j d + (k \oplus j)]N \tag{A5}$$

for all $j = 0, \ldots, d-1$. Furthermore, since N is an even number, $(-1)^{\sum_{i=1}^{d-1} m_i} = 1$ for all the Fock-states that have nonzero amplitudes in the code words. The code words thus take the form given in Eq. (1).

The setup and the error correction procedure that we investigate in this paper are given as follows (see Fig. 4). First, we prepare the logical state $\hat{\rho}$ in the two-mode encoding in the modes through which noise occurs $(\hat{a}_1, \hat{a}_2)$. Hence,

$$\bar{\hat{\rho}} = \sum_{i,j=0}^{1} \rho_{ij} |\bar{i}_N\rangle\langle\bar{j}_N|, \tag{A6}$$

where the bar denotes the logical code words in nontransformed basis, i.e., before the beam-splitter operation. Then, we apply the beam-splitter action,

$$\hat{U}_{\rm BS} = \exp[i\delta(\hat{G}^{+}_{12}\sin\phi + \hat{G}^{-}_{12}\cos\phi)] = \exp[\delta(\hat{a}_2^{\dagger}\hat{a}_1 e^{i\phi} - \hat{a}_1^{\dagger}\hat{a}_2 e^{-i\phi})], \tag{A7}$$

and let the system go through the noise channel $\mathcal{N} = \mathcal{N}_L \circ \mathcal{N}_D$, and then apply the inverse beam-splitter action $\hat{U}_{\rm BS}^{\dagger}$ before continuing with rest of the recovery operation, $\tilde{\mathcal{R}}$, where we have $\mathcal{R}(\bar{\hat{\rho}}) = \tilde{\mathcal{R}}(\hat{U}_{\rm BS}^{\dagger}\ \bar{\hat{\rho}}\ \hat{U}_{\rm BS})$. The beam-splitter transforms the two modes $\hat{a}_1$ and $\hat{a}_2$ into $\hat{b}_1$ and $\hat{b}_2$ as follows:

$$\begin{aligned}\hat{b}_1 &= \hat{U}_{\rm BS}^{\dagger}\hat{a}_1\hat{U}_{\rm BS} = \hat{a}_1\cos\delta + \hat{a}_2 e^{-i\phi}\sin\delta,\\ \hat{b}_2 &= \hat{U}_{\rm BS}^{\dagger}\hat{a}_2\hat{U}_{\rm BS} = \hat{a}_2\cos\delta - \hat{a}_1 e^{i\phi}\sin\delta.\end{aligned} \tag{A8}$$

With the Kraus representation provided in Eq. (8), the evolution of a state under these channels can be written as

$$\begin{aligned}\tilde{\mathcal{N}}(\bar{\hat{\rho}}) &= \hat{U}_{\rm BS}^{\dagger}\mathcal{N}(\hat{U}_{\rm BS}\bar{\hat{\rho}}\hat{U}_{\rm BS}^{\dagger})\hat{U}_{\rm BS}\\ &= \sum_{p,q,r,s=0}^{\infty} \hat{U}_{\rm BS}^{\dagger}\hat{L}_p^{(1)}\hat{L}_q^{(2)}\hat{D}_r^{(1)}\hat{D}_s^{(2)}\hat{U}_{\rm BS}\ \bar{\hat{\rho}}\ \hat{U}_{\rm BS}^{\dagger}\hat{D}_s^{(2)\dagger}\hat{D}_r^{(1)\dagger}\hat{L}_q^{(2)\dagger}\hat{L}_p^{(1)\dagger}\hat{U}_{\rm BS}.\end{aligned} \tag{A9}$$

Note that the modified noise channel under the beam-splitter operation is denoted by $\tilde{\mathcal{N}}$ instead of $\mathcal{N}$. We can further rewrite

$$\hat{U}_{\rm BS}^{\dagger}\hat{L}_p^{(1)}\hat{L}_q^{(2)}\hat{D}_r^{(1)}\hat{D}_s^{(2)}\hat{U}_{\rm BS} = \hat{\tilde{L}}_p^{(1)}\hat{\tilde{L}}_q^{(2)}\hat{\tilde{D}}_r^{(1)}\hat{\tilde{D}}_s^{(2)}, \tag{A10}$$

where, using Eq. (8), the Kraus operators are

$$\hat{\tilde{L}}_p^{(1)} = \sqrt{\frac{(1-e^{-\kappa_1 t})^p}{p!}}e^{-\frac{1}{2}\kappa_1 t\,\hat{b}_1^{\dagger}\hat{b}_1}\,\hat{b}_1^p, \quad \hat{\tilde{L}}_q^{(2)} = \sqrt{\frac{(1-e^{-\kappa_2 t})^q}{q!}}e^{-\frac{1}{2}\kappa_2 t\,\hat{b}_2^{\dagger}\hat{b}_2}\,\hat{b}_2^q, \tag{A11}$$

$$\hat{\tilde{D}}_r^{(1)} = \sqrt{\frac{(\gamma_1 t)^r}{r!}}e^{-\frac{1}{2}\gamma_1 t\,(\hat{b}_1^{\dagger}\hat{b}_1)^2}(\hat{b}_1^{\dagger}\hat{b}_1)^r, \quad \hat{\tilde{D}}_s^{(2)} = \sqrt{\frac{(\gamma_2 t)^s}{s!}}e^{-\frac{1}{2}\gamma_2 t\,(\hat{b}_2^{\dagger}\hat{b}_2)^2}(\hat{b}_2^{\dagger}\hat{b}_2)^s. \tag{A12}$$

The recovery procedure involves a nondestructive modular number measurement in the $(\hat{a}_1, \hat{a}_2)$ basis to detect the error syndrome and a corresponding unitary operator is applied. This modular number measurement in each of the modes is defined by the following set of positive operator-valued measures (POVMs): $\{\hat{\mathcal{P}}_{pq} = \hat{\mathcal{P}}_p \otimes \hat{\mathcal{P}}_q\}$, where $\hat{\mathcal{P}}_p := \sum_{m=0}^{\infty}|mN+p\rangle\langle mN+p|$ [13,15]. We intend to find the recovery map that corrects the error induced by the noise channel up to the first order in the noise strengths, $\kappa_i t$ and $\gamma_i t$, corresponding to the loss and dephasing channel, respectively. Up to the first order in $\kappa_i t$ and $\gamma_i t$, the effect of the noise channel can be written as

$$\begin{aligned}\tilde{\mathcal{N}}(\hat{\rho}) \approx \hat{\rho} &- \frac{\kappa_1 t}{2}\{\hat{b}_1^{\dagger}\hat{b}_1, \hat{\rho}\} - \frac{\kappa_2 t}{2}\{\hat{b}_2^{\dagger}\hat{b}_2, \hat{\rho}\} - \frac{\gamma_1 t}{2}\{(\hat{b}_1^{\dagger}\hat{b}_1)^2, \hat{\rho}\} - \frac{\gamma_2 t}{2}\{(\hat{b}_2^{\dagger}\hat{b}_2)^2, \hat{\rho}\} \\ &+ \kappa_1 t\;\hat{b}_1\hat{\rho}\hat{b}_1^{\dagger} + \kappa_2 t\;\hat{b}_2\hat{\rho}\hat{b}_2^{\dagger} + \gamma_1 t\;(\hat{b}_1^{\dagger}\hat{b}_1)\hat{\rho}(\hat{b}_1^{\dagger}\hat{b}_1) + \gamma_2 t\;(\hat{b}_2^{\dagger}\hat{b}_2)\hat{\rho}(\hat{b}_2^{\dagger}\hat{b}_2).\end{aligned} \tag{A13}$$

Based on this expansion, we give recovery procedures in the presence of purely loss and purely dephasing channels in Appendixes B and C, respectively, for general code words of our two-mode codes, corresponding to general f_{mn} in Eqs. (4) and (5).

APPENDIX B: RECOVERY OF THE TWO-MODE RSB CODE AGAINST THE LOSS CHANNEL UP TO FIRST ORDER IN NOISE STRENGTH

We rewrite the code words given in Eqs. (4) and (5) in the nontransformed basis, where the mixing operation $\hat{U}_{\rm BS}(\delta,\phi)$ has been absorbed into the error channel, as

$$|\bar{0}_N\rangle = \sum_{m,n} f_{mn}|2mN, (2n+1)N\rangle, \tag{B1}$$

$$|\bar{1}_N\rangle = \sum_{m,n} f_{mn}|(2n+1)N, 2mN\rangle. \tag{B2}$$

1. Knill-Laflamme conditions for purely loss channel

We now check the KL conditions for the loss channel up to first order in $\kappa_i t$. From Eq. (A11), the Kraus operators to first order in $\kappa_i t$ are

$$\hat{\tilde{L}}_0^{\prime(i)} = \left(\mathbb{I} - \tfrac{1}{2}\kappa_i t\hat{b}_i^{\dagger}\hat{b}_i\right), \quad \hat{\tilde{L}}_1^{\prime(i)} = \sqrt{\kappa_i t}\hat{b}_i. \tag{B3}$$

The corresponding error operators are

$$\hat{E}_1 = \hat{\tilde{L}}_0^{\prime(1)}\hat{\tilde{L}}_0^{\prime(2)}, \tag{B4}$$

$$\hat{E}_2 = \hat{\tilde{L}}_0^{\prime(1)}\hat{\tilde{L}}_1^{\prime(2)}, \tag{B5}$$

$$\hat{E}_3 = \hat{\tilde{L}}_1^{\prime(1)}\hat{\tilde{L}}_0^{\prime(2)}, \tag{B6}$$

$$\hat{E}_4 = \hat{\tilde{L}}_1^{\prime(1)}\hat{\tilde{L}}_1^{\prime(2)}. \tag{B7}$$

The KL conditions require

$$\langle\bar{i}_N|\hat{E}_a^{\dagger}\hat{E}_b|\bar{j}_N\rangle = C_{ab}\delta_{ij}, \tag{B8}$$

where $a,\ b = 1,\ 2,\ 3,\ 4$ and $i,\ j = 0,\ 1$. Among the ten possible combinations of $\hat{E}_a^{\dagger}\hat{E}_b$, three appear only at order higher than $(\kappa_i t)$ and can therefore be neglected. We evaluate the remaining seven cases below.

Case 1: $\hat{E}_1^{\dagger}\hat{E}_1$.

$$\hat{E}_1^{\dagger}\hat{E}_1 = \left(\mathbb{I} - \tfrac{1}{2}\kappa_1 t\hat{b}_1^{\dagger}\hat{b}_1\right)\left(\mathbb{I} - \tfrac{1}{2}\kappa_2 t\hat{b}_2^{\dagger}\hat{b}_2\right)\left(\mathbb{I} - \tfrac{1}{2}\kappa_1 t\hat{b}_1^{\dagger}\hat{b}_1\right)\left(\mathbb{I} - \tfrac{1}{2}\kappa_2 t\hat{b}_2^{\dagger}\hat{b}_2\right) \tag{B9}$$

$$= -\kappa_1 t \hat{b}_1^\dagger \hat{b}_1 - \kappa_2 t \hat{b}_2^\dagger \hat{b}_2 + \mathcal{O}((\kappa_i t)^2) \tag{B10}$$

$$= -\kappa_1 t(\cos^2\delta \hat{a}_1^\dagger \hat{a}_1 + \sin^2\delta \hat{a}_2^\dagger \hat{a}_2 + \sin\delta\cos\theta(e^{i\phi}\hat{a}_1^\dagger a_2 + e^{-i\phi}\hat{a}_2^\dagger a_1)) \tag{B11}$$

$$- \kappa_2 t(\cos^2\delta \hat{a}_2^\dagger \hat{a}_2 + \sin^2\delta \hat{a}_1^\dagger \hat{a}_1 + \sin\delta\cos\theta(-e^{i\phi}\hat{a}_1^\dagger a_2 + e^{-i\phi}\hat{a}_2^\dagger a_1)). \tag{B12}$$

For the code words in Eq. (B2), the off-diagonal matrix element is proportional to $\delta_{(2l+1)N,\ 2kN}\delta_{2mN+1,(2n+1)N-1}$, which is zero for $N \geqslant 2$ as required by KL conditions to be satisfied. Although we only consider even N, we note here that if $N = 1$, this matrix element will not vanish and thus not satisfying KL condition. Evaluating the diagonal terms yields

$$\langle \bar{0}_N|\hat{E}_1^\dagger \hat{E}_1|\bar{0}_N\rangle = -\kappa_1 t\left(\cos^2\delta \sum_{m,n}|f_{mn}|^2 2mN + \sin^2\delta \sum_{m,n}|f_{mn}|^2(2n+1)N\right)$$

$$-\kappa_2 t\left(\cos^2\delta \sum_{m,n}|f_{mn}|^2(2n+1)N + \sin^2\delta \sum_{m,n}|f_{mn}|^2 2mN\right), \tag{B13}$$

$$\langle \bar{1}_N|\hat{E}_1^\dagger \hat{E}_1|\bar{1}_N\rangle = -\kappa_1 t\left(\cos^2\delta \sum_{m,n}|f_{mn}|^2(2n+1)N + \sin^2\delta \sum_{m,n}|f_{mn}|^2 2mN\right)$$

$$-\kappa_2 t\left(\cos^2\delta \sum_{m,n}|f_{mn}|^2 2mN + \sin^2\delta \sum_{m,n}|f_{mn}|^2(2n+1)N\right). \tag{B14}$$

This leads to the condition

$$\cos^2\delta \sum_{m,n}|f_{mn}|^2(2mN - (2n+1)N) = \sin^2\delta \sum_{m,n}|f_{mn}|^2(2mN - (2n+1)N). \tag{B15}$$

Case 2: $\hat{E}_2^\dagger \hat{E}_1$.

$$\hat{E}_2^\dagger \hat{E}_1 = \sqrt{\kappa_2 t}\hat{b}_2^\dagger\left(\mathbb{I} - \tfrac{1}{2}\kappa_1 t \hat{b}_1^\dagger \hat{b}_1\right)\left(\mathbb{I} - \tfrac{1}{2}\kappa_1 t \hat{b}_1^\dagger \hat{b}_1\right)\left(\mathbb{I} - \tfrac{1}{2}\kappa_2 t \hat{b}_2^\dagger \hat{b}_2\right) \tag{B16}$$

$$= \sqrt{\kappa_2 t}\hat{b}_2^\dagger + \mathcal{O}((\kappa_i t)^2) \tag{B17}$$

$$= \sqrt{\kappa_2 t}(\hat{a}_1^\dagger \cos\delta - e^{-i\phi}\hat{a}_2^\dagger \sin\delta). \tag{B18}$$

Since $\langle \bar{i}_N|\hat{a}_{1,2}^\dagger|\bar{j}_N\rangle = 0$ for all i, j, the respective KL conditions are satisfied.

Case 3: $\hat{E}_3^\dagger \hat{E}_1$.

$$\hat{E}_3^\dagger \hat{E}_1 = \left(\mathbb{I} - \tfrac{1}{2}\kappa_1 t \hat{b}_2^\dagger \hat{b}_2\right)\sqrt{\kappa_1 t}\hat{b}_1^\dagger\left(\mathbb{I} - \tfrac{1}{2}\kappa_1 t \hat{b}_1^\dagger \hat{b}_1\right)\left(\mathbb{I} - \tfrac{1}{2}\kappa_2 t \hat{b}_2^\dagger \hat{b}_2\right) \tag{B19}$$

$$= \sqrt{\kappa_1 t}\hat{b}_1^\dagger + \mathcal{O}((\kappa_i t)^2). \tag{B20}$$

This produces the same operator structure as the previous case.

Case 4: $\hat{E}_4^\dagger \hat{E}_1$.

$$\hat{E}_4^\dagger \hat{E}_1 = \sqrt{\kappa_1 t}\sqrt{\kappa_2 t}\hat{b}_2^\dagger \hat{b}_1^\dagger\left(\mathbb{I} - \tfrac{1}{2}\kappa_1 t \hat{b}_1^\dagger \hat{b}_1\right)\left(\mathbb{I} - \tfrac{1}{2}\kappa_2 t \hat{b}_2^\dagger \hat{b}_2\right)$$

$$= \sqrt{\kappa_1 t}\sqrt{\kappa_2 t}\hat{b}_2^\dagger \hat{b}_1^\dagger + \mathcal{O}((\kappa_i t)^2)$$

$$= \sqrt{\kappa_1 t}\sqrt{\kappa_2 t}(\hat{a}_1^\dagger \hat{a}_2^\dagger(\cos^2\delta - \sin^2\delta) + (\hat{a}_2^\dagger \hat{a}_2^\dagger e^{i\phi} - \hat{a}_1^\dagger \hat{a}_1^\dagger e^{-i\phi})\sin\delta\cos\delta). \tag{B21}$$

For all error operators appearing here, we have $\langle \bar{i}_N|\hat{a}_1^\dagger \hat{a}_1^\dagger|\bar{j}_N\rangle = \langle \bar{i}_N|\hat{a}_2^\dagger \hat{a}_2^\dagger|\bar{j}_N\rangle = \langle \bar{i}_N|\hat{a}_1^\dagger \hat{a}_2^\dagger|\bar{j}_N\rangle = 0$ for all pairs i, j.

Case 5: $\hat{E}_2^\dagger \hat{E}_2$.

$$\hat{E}_2^\dagger \hat{E}_2 = \kappa_2 t \hat{b}_2^\dagger \hat{b}_2 + \mathcal{O}((\kappa_i t)^2). \tag{B22}$$

This yields the same condition as obtained from $\hat{E}_1^\dagger \hat{E}_1$.

Case 6: $\hat{E}_3^\dagger \hat{E}_2$.

$$\hat{E}_3^\dagger \hat{E}_2 = \left(\mathbb{I} - \tfrac{1}{2}\kappa_2 t \hat{b}^\dagger \hat{b}\right)\sqrt{\kappa_1 t}\hat{b}_1^\dagger\left(\mathbb{I} - \tfrac{1}{2}\kappa_1 t \hat{b}_1 \dagger \hat{b}_1\right)\sqrt{\kappa_2 t}\hat{b}_2 \tag{B23}$$

$$= \sqrt{\kappa_1 \kappa_2}t \hat{b}_1^\dagger \hat{b}_2 + \mathcal{O}((\kappa_i t)^2) \tag{B24}$$

$$= \sqrt{\kappa_1 \kappa_2}t(\hat{a}_2^\dagger \hat{a}_2 e^{i\theta}\sin\delta\cos\delta - \hat{a}_1^\dagger \hat{a}_1 e^{i\theta}\sin\delta\cos\delta + \hat{a}_1^\dagger \hat{a}_2\cos^2\delta - \hat{a}_2^\dagger \hat{a}_1\sin^2\delta). \tag{B25}$$

Evaluating the diagonal matrix elements gives

$$\langle \bar{0}_N|\hat{E}_3^\dagger \hat{E}_2|\bar{0}_N\rangle = \sqrt{\kappa_1\kappa_2}t \sum_{m,n} |f_{mn}|^2(2mN-(2n+1)N)e^{i\theta}\sin\delta\cos\delta, \tag{B26}$$

$$\langle \bar{1}_N|\hat{E}_3^\dagger \hat{E}_2|\bar{1}_N\rangle = \sqrt{\kappa_1\kappa_2}t \sum_{m,n} |f_{mn}|^2((2n+1)N-2mN)e^{i\theta}\sin\delta\cos\delta. \tag{B27}$$

Thus, for the KL condition to be satisfied, if $\delta \neq 0$ we require $\sum_{m,n}|f_{mn}|^2(2mN-(2n+1)N)=0$.

Case 7: $\hat{E}_3^\dagger\hat{E}_3$.

$$\hat{E}_3^\dagger\hat{E}_3 = \kappa_1 t\hat{b}_1^\dagger\hat{b}_1 + \mathcal{O}((\kappa_i t)^2). \tag{B28}$$

This produces the same constraint as in the $\hat{E}_1^\dagger\hat{E}_1$ case.

Conclusion: Collecting the above results, the KL conditions for the loss channel to the first order in loss parameter require

$$\boxed{\sum_{m,n}|f_{mn}|^2(m-n)=\frac{1}{2}}. \tag{B29}$$

Notably, the binomial instances with $N \geqslant 2$ and $K=2$ satisfy this condition.

2. Recovery map for purely loss channel

From Eq. (A13), we see that in the presence of only the loss channel, the state evolution up to first order in the noise strength is given by

$$\tilde{\mathcal{N}}_L(\bar{\rho}) \approx \bar{\rho} - \frac{\kappa_1 t}{2}\{\hat{b}_1^\dagger\hat{b}_1,\bar{\rho}\} - \frac{\kappa_2 t}{2}\{\hat{b}_2^\dagger\hat{b}_2,\bar{\rho}\} + \kappa_1 t\ \hat{b}_1\bar{\rho}\hat{b}_1^\dagger + \kappa_2 t\ \hat{b}_2\bar{\rho}\hat{b}_2^\dagger. \tag{B30}$$

For the code words given in Eq. (B2), we define the projector onto the code space as $\hat{P}_C = |\bar{0}_N\rangle\langle\bar{0}_N| + |\bar{1}_N\rangle\langle\bar{1}_N|$. We now recall the modular measurement POVM defined as

$$\{\hat{\mathcal{P}}_{00},\hat{\mathcal{P}}_{01},\hat{\mathcal{P}}_{10},(\mathbb{I}-\hat{\mathcal{P}}_{00}-\hat{\mathcal{P}}_{01}-\hat{\mathcal{P}}_{10})\},$$

where $\hat{\mathcal{P}}_{pq} = \hat{\mathcal{P}}_p \otimes \hat{\mathcal{P}}_q$ and $\hat{\mathcal{P}}_p = \sum_m |mN+p\rangle\langle mN+p|$.

Applying this measurement projects the noisy state onto different error syndromes, corresponding to no-jump or photon loss in each mode. We now analyze the resulting state and recovery operation for each syndrome.

(1) *Syndrome* $(p,q)=(0,0)$. If the measurement outcome corresponds to no-jump $\hat{\mathcal{P}}_{00}$, the projected state becomes

$$\hat{\mathcal{P}}_{00}\tilde{\mathcal{N}}_L(\bar{\rho})\hat{\mathcal{P}}_{00}^\dagger = \bar{\rho} - \{\hat{M}_0^L,\bar{\rho}\}, \tag{B31}$$

where $\hat{M}_0^L = A\hat{a}_1^\dagger\hat{a}_1 + B\hat{a}_2^\dagger\hat{a}_2$, with $A=\frac{1}{2}(\kappa_1 t\cos^2\delta+\kappa_2 t\sin^2\delta)$ and $B=\frac{1}{2}(\kappa_2 t\cos^2\delta+\kappa_1 t\sin^2\delta)$.

To correct this error, we apply the unitary

$$\hat{U}_{00}^L = \exp\left([\hat{M}_0^L,\hat{P}_C]\right). \tag{B32}$$

The superscript L corresponds to unitaries for loss noise correction and D in the next Appendix will correspond to unitaries for dephasing noise correction. The action of this operation gives

$$\begin{aligned}\hat{U}_{00}^L\hat{\mathcal{P}}_{00}\tilde{\mathcal{N}}_L(\bar{\rho})\hat{\mathcal{P}}_{00}^\dagger\hat{U}_{00}^{L\dagger} &= \left(\mathbb{I}^{\otimes 2}+[\hat{M}_0^L,\hat{P}_C]\right)\left(\bar{\rho}-\{\hat{M}_0^L,\bar{\rho}\}\right)\left(\mathbb{I}^{\otimes 2}-[\hat{M}_0^L,\hat{P}_C]\right)\\ &= \bar{\rho}-\{\hat{M}_0^L,\bar{\rho}\}+[\hat{M}_0^L,\hat{P}_C]\bar{\rho}-\bar{\rho}[\hat{M}_0^L,\hat{P}_C]\\ &= \bar{\rho}-\{\hat{P}_C\hat{M}_0^L\hat{P}_C,\bar{\rho}\}\\ &= \bar{\rho}-2\alpha^2N(A+B)\bar{\rho},\end{aligned} \tag{B33}$$

where we used the equality implied by the KL condition

$$\alpha^2N = \sum_{m,n}|f_{mn}|^2 2mN = \sum_{m,n}|f_{mn}|^2(2n+1)N.$$

We also used that $\hat{P}_C\bar{\rho}=\bar{\rho}$ and $\langle\bar{i}_N|\hat{M}_0^L|\bar{j}_N\rangle \propto \delta_{ij}$.

(2) *Syndrome* $(p,q)=(0,1)$.

If the measurement outcome corresponds to $\hat{\mathcal{P}}_{01}$, the projected state becomes

$$\hat{\mathcal{P}}_{01}\tilde{\mathcal{N}}_L(\bar{\rho})\hat{\mathcal{P}}_{01}^\dagger = 2B\hat{a}_2\bar{\rho}\hat{a}_2^\dagger. \tag{B34}$$

We then apply the unitary

$$\hat{U}_{01}^{L} = |\bar{0}_N\rangle\langle\bar{0}_E|^{(2)} + |\bar{1}_N\rangle\langle\bar{1}_E|^{(2)}, \tag{B35}$$

where

$$|\bar{i}_E\rangle^{(r)} = \frac{\hat{a}_r|\bar{i}_N\rangle}{\sqrt{\alpha^2 N}}. \tag{B36}$$

Here, $\|\hat{a}_j|\bar{i}_N\rangle\| = \sqrt{\alpha^2 N}$ is the norm and $i \in \{0, 1\}$ and where $r \in \{1, 2\}$. Here, we used the KL condition $\langle\bar{i}_N|\hat{a}_r^\dagger\hat{a}_r|\bar{i}_N\rangle = \alpha^2 N$. Applying the recovery operation yields

$$\begin{aligned}
\hat{U}_{01}^{L}\hat{\mathcal{P}}_{01}\tilde{\mathcal{N}}_L(\bar{\rho})\hat{\mathcal{P}}_{01}^{\dagger}\hat{U}_{01}^{L\dagger} &= (|\bar{0}_N\rangle\langle\bar{0}_E|^{(2)} + |\bar{1}_N\rangle\langle\bar{1}_E|^{(2)})(2B\hat{a}_2\bar{\rho}\hat{a}_2^\dagger)(|\bar{0}_E\rangle^{(2)}\langle\bar{0}_N| + |\bar{1}_E\rangle^{(2)}\langle\bar{1}_N|) \\
&= 2B(|\bar{0}_N\rangle\langle\bar{0}_E|^{(2)} + |\bar{1}_N\rangle\langle\bar{1}_E|^{(2)})\left(\sum_{i,j}\alpha^2 N\rho_{ij}|\bar{i}_E\rangle\langle\bar{j}_E|^{(2)}\right)(|\bar{0}_E\rangle^{(2)}\langle\bar{0}_N| + |\bar{1}_E\rangle^{(2)}\langle\bar{1}_N|) \\
&= 2B\alpha^2 N\left(\sum_{i,j}\rho_{i,j}|\bar{i}_N\rangle\langle\bar{j}_N|\right) \\
&= 2B\alpha^2 N\bar{\rho},
\end{aligned} \tag{B37}$$

(3) *Syndrome* $(p, q) = (1, 0)$.

Similarly, if the outcome corresponds to $\hat{\mathcal{P}}_{01}$, we obtain

$$\hat{\mathcal{P}}_{01}\tilde{\mathcal{N}}_L(\bar{\rho})\hat{\mathcal{P}}_{01}^{\dagger} = 2A\hat{a}_1\bar{\rho}\hat{a}_1^\dagger \tag{B38}$$

and apply the unitary

$$\hat{U}_{10}^{L} = |\bar{0}_N\rangle\langle\bar{0}_E|^{(1)} + |\bar{1}_N\rangle\langle\bar{1}_E|^{(1)}. \tag{B39}$$

Analogously,

$$\hat{U}_{10}^{L}\hat{\mathcal{P}}_{10}\tilde{\mathcal{N}}_L(\bar{\rho})\hat{\mathcal{P}}_{10}^{\dagger}\hat{U}_{10}^{L\dagger} = 2A\alpha^2 N. \tag{B40}$$

If the measurement outcome corresponds to $(\mathbb{I} - \hat{\mathcal{P}}_{00} - \hat{\mathcal{P}}_{01} - \hat{\mathcal{P}}_{10})$, we perform no correction since it corresponds to a second-order error.

Thus, the recovery channel is

$$\tilde{\mathcal{R}} \sim \left\{\hat{U}_{00}^{L}\hat{\mathcal{P}}_{00}, \hat{U}_{01}^{L}\hat{\mathcal{P}}_{01}, \hat{U}_{10}^{L}\hat{\mathcal{P}}_{10}, (\mathbb{I} - \hat{\mathcal{P}}_{00} - \hat{\mathcal{P}}_{01} - \hat{\mathcal{P}}_{10})\right\}. \tag{B41}$$

Summing Eqs. (B33), (B37), and (B40) yields

$$\tilde{\mathcal{R}} \circ \tilde{\mathcal{N}}_L(\bar{\rho}) = \bar{\rho} + \mathcal{O}((\kappa_i t)^2). \tag{B42}$$

APPENDIX C: RECOVERY THE TWO-MODE RSB CODE AGAINST DEPHASING CHANNEL UP TO FIRST ORDER IN NOISE STRENGTH

1. Knill-Laflamme conditions for purely dephasing channel

We now check the KL conditions for the two-mode code under a purely dephasing channel up to first order in $\gamma_i t$.

From Eq. (A12), the error operators up to first order are

$$\hat{\tilde{D}}_0^{\prime(i)} = \mathbb{I} - \tfrac{1}{2}\gamma_i t(\hat{b}_i^\dagger\hat{b}_i)^2, \tag{C1}$$

$$\hat{\tilde{D}}_1^{\prime(i)} = \sqrt{\gamma_i t}\hat{b}_i^\dagger\hat{b}_i. \tag{C2}$$

The combined two-mode error operators are

$$\hat{E}_1 = \hat{\tilde{D}}_0^{\prime(1)}\hat{\tilde{D}}_0^{\prime(2)}, \tag{C3}$$

$$\hat{E}_2 = \hat{\tilde{D}}_0^{\prime(1)}\hat{\tilde{D}}_1^{\prime(2)}, \tag{C4}$$

$$\hat{E}_3 = \hat{\tilde{D}}_1^{\prime(1)}\hat{\tilde{D}}_0^{\prime(2)}, \tag{C5}$$

$$\hat{E}_4 = \hat{\tilde{D}}_1^{\prime(1)}\hat{\tilde{D}}_1^{\prime(2)}. \tag{C6}$$

The KL condition requires

$$\langle \bar{i}_N|\hat{E}_a^\dagger \hat{E}_b|\bar{j}_N\rangle = C_{ab}\delta_{ij}, \quad a,b=1,\ldots,4,\ i,j=0,1. \tag{C7}$$

We now evaluate each relevant combination up to first order in $\gamma_i t$.

Case 1: $\hat{E}_1^\dagger \hat{E}_1$.

$$\hat{E}_1^\dagger \hat{E}_1 = \big(\mathbb{I} - \tfrac{1}{2}\gamma_1 t(\hat{b}_1^\dagger \hat{b}_1)^2\big)\big(\mathbb{I} - \tfrac{1}{2}\gamma_2 t(\hat{b}_2^\dagger \hat{b}_2)^2\big)\big(\mathbb{I} - \tfrac{1}{2}\gamma_1 t(\hat{b}_1^\dagger \hat{b}_1)^2\big)\big(\mathbb{I} - \tfrac{1}{2}\gamma_2 t(\hat{b}_2^\dagger \hat{b}_2)^2\big) \tag{C8}$$

$$= -\gamma_1 t(\hat{b}_1^\dagger \hat{b}_1)^2 - \gamma_2 t(\hat{b}_2^\dagger \hat{b}_2)^2 + \mathcal{O}((\gamma_i t)^2) \tag{C9}$$

$$\begin{aligned} &= -\gamma_1 t[(\cos^2\delta \hat{a}_1^\dagger \hat{a}_1 + \sin^2\delta \hat{a}_2^\dagger \hat{a}_2)^2 + \sin^2\delta\cos^2\delta(e^{i\phi}\hat{a}_1^\dagger \hat{a}_2 + e^{-i\phi}\hat{a}_2^\dagger \hat{a}_1)^2] \\ &\quad - \gamma_2 t[(\cos^2\delta \hat{a}_2^\dagger \hat{a}_2 + \sin^2\delta \hat{a}_1^\dagger \hat{a}_1)^2 + \sin^2\delta\cos^2\delta(-e^{i\phi}\hat{a}_1^\dagger \hat{a}_2 + e^{-i\phi}\hat{a}_2^\dagger \hat{a}_1)^2] + \text{cross terms}. \end{aligned} \tag{C10}$$

For the KL condition, cross terms with unequal numbers of operators in each mode vanish. The diagonal elements give

$$\begin{aligned} \langle \bar{0}_N|\hat{E}_1^\dagger \hat{E}_1|\bar{0}_N\rangle &= -\gamma_1 t \sum_{m,n} |f_{mn}|^2 (2mN\cos^2\delta + (2n+1)N\sin^2\delta)^2 \\ &\quad - \gamma_2 t \sum_{m,n} |f_{mn}|^2 ((2n+1)N\cos^2\delta + 2mN\sin^2\delta)^2 \\ &\quad - (\gamma_1+\gamma_2)t\sin^2\delta\cos^2\delta \sum_{m,n} |f_{mn}|^2 (2mN((2n+1)N+1) + ((2mN+1)(2n+1)N)), \end{aligned} \tag{C11}$$

$$\begin{aligned} \langle \bar{1}_N|\hat{E}_1^\dagger \hat{E}_1|\bar{1}_N\rangle &= -\gamma_1 t \sum_{m,n} |f_{mn}|^2 ((2n+1)N\cos^2\delta + 2mN\sin^2\delta)^2 \\ &\quad - \gamma_2 t \sum_{m,n} |f_{mn}|^2 (2mN\cos^2\delta + (2n+1)N\sin^2\delta)^2 \\ &\quad - (\gamma_1+\gamma_2)t\sin^2\delta\cos^2\delta \sum_{m,n} |f_{mn}|^2 (2mN((2n+1)N+1) + ((2mN+1)(2n+1)N)). \end{aligned} \tag{C12}$$

Equating these gives the condition

$$\delta = \pi/4 \quad \text{or} \quad \sum_{m,n} |f_{mn}|^2 (2m)^2 = \sum_{m,n} |f_{mn}|^2 (2n+1)^2. \tag{C13}$$

Off-diagonal terms for $i \neq j$ are reduced to $\langle \bar{i}_N|\hat{E}_1^\dagger \hat{E}_1|\bar{j}_N\rangle$. This is proportional to $\propto \langle \bar{i}_N|(\pm e^{i\phi}\hat{a}_1^\dagger a_2 + e^{-i\phi}\hat{a}_2^\dagger a_1)^2|\bar{j}_N\rangle = 0$ for $N \geqslant 4$.

Case 2: $\hat{E}_2^\dagger \hat{E}_1$.

$$\hat{E}_2^\dagger \hat{E}_1 = \sqrt{\gamma_2 t}\hat{b}_2^\dagger \hat{b}_2\big(\mathbb{I} - \tfrac{1}{2}\gamma_1 t(\hat{b}_1^\dagger \hat{b}_1)^2\big)^2\big(\mathbb{I} - \tfrac{1}{2}\gamma_2 t(\hat{b}_2^\dagger \hat{b}_2)^2\big) \tag{C14}$$

$$= \sqrt{\gamma_2 t}\hat{b}_2^\dagger \hat{b}_2 + \mathcal{O}((\gamma_i t)^2) \tag{C15}$$

$$= \sqrt{\gamma_2 t}(\cos^2\delta \hat{a}_2^\dagger \hat{a}_2 + \sin^2\delta \hat{a}_1^\dagger \hat{a}_1 - \sin\delta\cos\delta(e^{-i\phi}\hat{a}_2^\dagger \hat{a}_1 + e^{i\phi}\hat{a}_2^\dagger \hat{a}_1)). \tag{C16}$$

Diagonal elements give the same δ condition as Case 1; off-diagonal terms vanish for any δ, ϕ, and f_{mn}.

Case 3: $\hat{E}_3^\dagger \hat{E}_1$.

$$\hat{E}_3^\dagger \hat{E}_1 = \sqrt{\gamma_1 t}\hat{b}_1^\dagger \hat{b}_1\big(\mathbb{I} - \tfrac{1}{2}\gamma_2 t(\hat{b}_2^\dagger \hat{b}_2)^2\big)\big(\mathbb{I} - \tfrac{1}{2}\gamma_1 t(\hat{b}_1^\dagger \hat{b}_1)^2\big)\big(\mathbb{I} - \tfrac{1}{2}\gamma_2 t(\hat{b}_2^\dagger \hat{b}_2)^2\big) \tag{C17}$$

$$= \sqrt{\gamma_1 t}\hat{b}_1^\dagger \hat{b}_1 + \mathcal{O}((\gamma_i t)^2), \tag{C18}$$

which is analogous to Case 2.

Case 4: $\hat{E}_4^\dagger \hat{E}_1$.

$$\begin{aligned} \hat{E}_4^\dagger \hat{E}_1 &= \sqrt{\gamma_1\gamma_2}t\hat{b}_2^\dagger \hat{b}_2 \hat{b}_1^\dagger \hat{b}_1\big(\mathbb{I} - \tfrac{1}{2}\gamma_2 t(\hat{b}_2^\dagger \hat{b}_2)^2\big)\big(\mathbb{I} - \tfrac{1}{2}\gamma_1 t(\hat{b}_1^\dagger \hat{b}_1)^2\big) \\ &= \sqrt{\gamma_1\gamma_2}t\hat{b}_2^\dagger \hat{b}_2 \hat{b}_1^\dagger \hat{b}_1 + \mathcal{O}((\kappa_i t)^2) \\ &= \sqrt{\gamma_1\gamma_2}t(\cos^2\delta \hat{a}_2^\dagger \hat{a}_2 + \sin^2\delta \hat{a}_1^\dagger \hat{a}_1 + \sin\delta\cos\delta(-e^{i\phi}\hat{a}_1^\dagger a_2 + e^{-i\phi}\hat{a}_2^\dagger a_1)) \\ &\quad \times (\cos^2\delta \hat{a}_1^\dagger \hat{a}_1 + \sin^2\delta \hat{a}_2^\dagger \hat{a}_2 + \sin\delta\cos\delta(e^{i\phi}\hat{a}_1^\dagger a_2 + e^{-i\phi}\hat{a}_2^\dagger a_1)). \end{aligned} \tag{C19}$$

For the diagonal entries, we get

$$\langle \bar{0}_N|\hat{E}_4^\dagger \hat{E}_1|\bar{0}_N\rangle = \langle \bar{1}_N|\hat{E}_4^\dagger \hat{E}_1|\bar{1}_N\rangle = \sqrt{\gamma_1\gamma_2}t(C^2 + 2\alpha^2 N), \tag{C20}$$

where $C^2 = \sum_{m,n} |f_{mn}|^2((2mN)^2 + ((2n+1)N)^2)$ and, as defined before, $\alpha^2 N = \sum_{m,n} |f_{mn}|^2 2mN = \sum_{m,n} |f_{mn}|^2 (2n+1)N$. Further, we see that the off diagonals $\langle \bar{0}_N | \hat{E}_4^\dagger \hat{E}_1 | \bar{1}_N \rangle = 0$.

Cases 5–7: $\hat{E}_2^\dagger \hat{E}_2$, $\hat{E}_3^\dagger \hat{E}_2$, $\hat{E}_3^\dagger \hat{E}_3$.

For these cases, we see that $\hat{E}_2^\dagger \hat{E}_2$, $\hat{E}_3^\dagger \hat{E}_2$, and $\hat{E}_3^\dagger \hat{E}_3$ are similar to Case 1, Case 4, and Case 5, respectively. They give the same diagonal conditions as Case 1 and the off-diagonal terms vanish.

Conclusion: For KL conditions to be satisfied up to first order in noise strength, we require that $N \geqslant 4$ and

$$\boxed{\delta = \pi/4} \quad \text{or} \quad \boxed{\sum_{m,n} |f_{mn}|^2 (m^2 - n^2 - n) = \frac{1}{4}}. \tag{C21}$$

We note that the KL conditions for second order in noise strength $\kappa_i t$ are not satisfied.

2. Recovery map for purely dephasing channel

From Eq. (A13), we see that in the presence of a purely dephasing channel, the state evolution up to first order in the noise strength is given by

$$\tilde{\mathcal{N}}_D(\bar{\rho}) \approx \bar{\rho} - \frac{\gamma_1 t}{2}\{(\hat{b}_1^\dagger \hat{b}_1)^2, \bar{\rho}\} - \frac{\gamma_2 t}{2}\{(\hat{b}_2^\dagger \hat{b}_2)^2, \bar{\rho}\} + \gamma_1 t\ (\hat{b}_1^\dagger \hat{b}_1)\bar{\rho}(\hat{b}_1^\dagger \hat{b}_1) + \gamma_2 t\ (\hat{b}_2^\dagger \hat{b}_2)\bar{\rho}(\hat{b}_2^\dagger \hat{b}_2). \tag{C22}$$

We employ the following modular measurement,

$$\{\hat{\mathcal{P}}_{00}, \hat{\mathcal{P}}_{-1,1}, \hat{\mathcal{P}}_{1,-1}, (\mathbb{I} - \hat{\mathcal{P}}_{00} - \hat{\mathcal{P}}_{1,-1} - \hat{\mathcal{P}}_{-1,1})\}.$$

Applying this measurement projects the noisy state onto different error syndromes corresponding to either no jump or photon exchange between the two modes. For the no-jump component, we will see that an additional projective measurement is required for full recovery.

Since the modular measurements are performed in the nontransformed mode basis—chosen for experimental feasibility in microwave cavities—we still require the following condition to hold, even for a purely dephasing channel:

$$\sum_{m,n} |f_{mn}|^2 2mN = \sum_{m,n} |f_{mn}|^2 (2n+1)N.$$

This condition ensures that the recovery map described below remains valid.

We note, however, that for a purely dephasing channel the KL conditions are always satisfied when $\delta = \pi/4$. Therefore, there should exist an appropriate basis in which the recovery map can be constructed without imposing this additional constraint. Nevertheless, since the above condition coincides with the one obtained from the KL analysis of the loss channel, it is convenient to employ the same family of codes for both noise processes. With this choice, the recovery map presented below applies directly to the dephasing case as well.

(1) *Syndrome* $(p, q) = (0, 0)$.

If the measurement outcome corresponds to the no-jump event $\hat{\mathcal{P}}_{00}$, the projected state becomes

$$\hat{\mathcal{P}}_{00}\tilde{\mathcal{N}}_D(\bar{\rho})\hat{\mathcal{P}}_{00}^\dagger = \bar{\rho} - \{\hat{M}_0^D, \bar{\rho}\} + \hat{M}_1^D \bar{\rho} \hat{M}_1^{D\dagger}. \tag{C23}$$

Here,

$$\hat{M}_0^D = \frac{(\gamma_1 + \gamma_2)t}{8}[(\hat{a}_1^\dagger \hat{a}_1 + \hat{a}_2^\dagger \hat{a}_2)^2 + \hat{a}_2^\dagger \hat{a}_1 \hat{a}_1^\dagger \hat{a}_2 + \hat{a}_1^\dagger \hat{a}_2 \hat{a}_2^\dagger \hat{a}_1]$$

and

$$\hat{M}_1^D = \frac{\sqrt{(\gamma_1 + \gamma_2)t}}{2}(\hat{a}_1^\dagger \hat{a}_1 + \hat{a}_2^\dagger \hat{a}_2).$$

To correct the first term, we apply the unitary

$$\hat{U}_{00}^D = \exp\left([\hat{M}_0^D, \hat{P}_C]\right). \tag{C24}$$

The action of this operation yields, up to $O(\gamma_i t)$,

$$\begin{aligned}
\hat{U}_{00}^D \hat{\mathcal{P}}_{00}\tilde{\mathcal{N}}_D(\bar{\rho})\hat{\mathcal{P}}_{00}^\dagger \hat{U}_{00}^{D\dagger} &= \left(\mathbb{I}^{\otimes 2} + [\hat{M}_0^D, \hat{P}_C]\right)\left(\bar{\rho} - \{\hat{M}_0^D, \bar{\rho}\} + \hat{M}_1^D \bar{\rho} \hat{M}_1^{D\dagger}\right)\left(\mathbb{I}^{\otimes 2} - [\hat{M}_0^D, \hat{P}_C]\right) \\
&= \bar{\rho} - \{\hat{P}_C \hat{M}_0^D \hat{P}_C, \bar{\rho}\} + \hat{M}_1^D \bar{\rho} \hat{M}_1^{D\dagger} \\
&= \bar{\rho} - \frac{(\gamma_1 + \gamma_2)t}{4}(4\beta_0^2 + C^2 + \alpha^2 N)\bar{\rho} + \hat{M}_1^D \bar{\rho} \hat{M}_1^{D\dagger}.
\end{aligned} \tag{C25}$$

In deriving this expression, we used

$$\langle \bar{0}_N | \hat{M}_0^D | \bar{0}_N \rangle = \langle \bar{1}_N | \hat{M}_0^D | \bar{1}_N \rangle = C^2 + 4\beta_0^2 + 2\alpha^2 N,$$

where we defined

$$\beta^2 = \sum_{m,n} |f_{mn}|^2\, 2m(2n+1)N^2.$$

To correct the remaining term $\hat{M}_1^D \bar{\tilde{\rho}} \hat{M}_1^{D\dagger}$, we perform an additional projective measurement

$$\hat{P}_{CE} = \{\hat{P}_C + \hat{P}_1', \hat{P}_E + \hat{P}_2'\},$$

where

$$\hat{P}_E = |\bar{0}\rangle_E^{\perp}\langle\bar{0}|_E^{\perp} + |\bar{1}\rangle_E^{\perp}\langle\bar{1}|_E^{\perp}. \tag{C26}$$

Here, we have defined the orthogonal states

$$|\bar{i}\rangle_E^{\perp} = (\hat{a}_1^\dagger \hat{a}_1 + \hat{a}_2^\dagger \hat{a}_2)|\bar{i}_N\rangle,$$

which can be written as

$$|\bar{i}\rangle_E^{\perp} = \frac{1}{\sqrt{C_2 - C_1^2}}(C_1|\bar{i}_N\rangle - |\bar{i}\rangle_E). \tag{C27}$$

where $C_1 = \langle\bar{0}_N|(\hat{a}_1^\dagger\hat{a}_1 + \hat{a}_2^\dagger\hat{a}_2)|\bar{0}_N\rangle = \langle\bar{1}_N|(\hat{a}_1^\dagger\hat{a}_1 + \hat{a}_2^\dagger\hat{a}_2)|\bar{1}_N\rangle = 2\alpha^2 N$ and $C_2 = \langle\bar{0}_N|(\hat{a}_1^\dagger\hat{a}_1 + \hat{a}_2^\dagger\hat{a}_2)^2|\bar{0}_N\rangle = \langle\bar{1}_N|(\hat{a}_1^\dagger\hat{a}_1 + \hat{a}_2^\dagger\hat{a}_2)^2|\bar{1}_N\rangle = \sum_{m,n}|f_{mn}|^2((2mN)^2 + ((2n+1)N)^2 + 4m(2n+1)N^2 = C^2 + 2\beta_0^2$. This ensures the states are correctly normalized. The projectors $\hat{P}_i'$ above are complementary projectors to ensure that the POVMs sum to identity.

If the measurement outcome corresponds to $\hat{P}_C$ we do nothing, while for the $\hat{P}_E$ outcome we apply

$$\hat{U}_E^D = |\bar{0}_N\rangle\langle\bar{0}_E|^{\perp} + |\bar{1}_N\rangle\langle\bar{1}_E|^{\perp}.$$

The action of these operators on the term $\hat{M}_1^D \bar{\tilde{\rho}} \hat{M}_1^{D\dagger}$ is

$$\hat{P}_C \hat{M}_1^D \bar{\tilde{\rho}} \hat{M}_1^{D\dagger} \hat{P}_C + \hat{U}_E^D \hat{P}_E \hat{M}_1^D \bar{\tilde{\rho}} \hat{M}_1^{D\dagger} \hat{P}_E \hat{U}_E^{D\dagger} = \frac{(\gamma_1+\gamma_2)t}{4}(C^2 + 2\beta_0^2)\bar{\tilde{\rho}}. \tag{C28}$$

Combining the above results, the contribution from the no-jump sector becomes

$$\begin{aligned}
&\hat{P}_C \hat{U}_{00}^D \hat{\mathcal{P}}_{00} \tilde{\mathcal{N}}_D(\bar{\tilde{\rho}}) \hat{\mathcal{P}}_{00}^\dagger \hat{U}_{00}^{D\dagger} \hat{P}_C + \hat{U}_E^D \hat{P}_E \hat{U}_{00}^D \hat{\mathcal{P}}_{00} \tilde{\mathcal{N}}_D(\bar{\tilde{\rho}}) \hat{\mathcal{P}}_{00}^\dagger \hat{U}_{00}^{D\dagger} \hat{P}_E \hat{U}_E^{D\dagger} \\
&= \bar{\tilde{\rho}} + \frac{(\gamma_1+\gamma_2)t}{4}\big(-4\beta_0^2 - C^2 - 2\alpha^2 N + C^2 + 2\beta_0^2\big) \\
&= \bar{\tilde{\rho}} + \frac{(\gamma_1+\gamma_2)t}{4}\big(-2\beta_0^2 - 2\alpha^2 N\big).
\end{aligned} \tag{C29}$$

(2) *Syndrome* $(p, q) = (1, -1)$.

If the measurement outcome corresponds to a photon exchange with gain in the first mode and loss in the second mode, the projected state becomes

$$\hat{\mathcal{P}}_{1,-1} \tilde{\mathcal{N}}_D(\bar{\tilde{\rho}}) \hat{\mathcal{P}}_{1,-1}^\dagger = \frac{(\gamma_1+\gamma_2)t}{4}(\hat{a}_1^\dagger \hat{a}_2 \bar{\tilde{\rho}} \hat{a}_2^\dagger \hat{a}_1). \tag{C30}$$

To correct this error, we apply the unitary

$$\hat{U}_{1,-1} = |\bar{0}_N\rangle\langle\bar{0}|_{1,-1} + |\bar{1}_N\rangle\langle\bar{1}|_{1,-1}. \tag{C31}$$

Here,

$$|\bar{i}\rangle_{1,-1} = \frac{1}{\sqrt{\beta}}(\hat{a}_1^\dagger \hat{a}_2)|\bar{i}_N\rangle,$$

with

$$\beta = \beta_0^2 + \alpha^2 N.$$

The action of the recovery operation then gives

$$\hat{U}_{1,-1} \hat{\mathcal{P}}_{1,-1} \tilde{\mathcal{N}}_D(\bar{\tilde{\rho}}) \hat{\mathcal{P}}_{1,-1}^\dagger \hat{U}_{1,-1}^\dagger = \frac{(\gamma_1+\gamma_2)t}{4}(\beta_0^2 + \alpha^2 N)\bar{\tilde{\rho}}. \tag{C32}$$

(3) *Syndrome* $(p, q) = (-1, 1)$.

For this outcome, the projected state is

$$\hat{\mathcal{P}}_{-1,1} \tilde{\mathcal{N}}_D(\bar{\tilde{\rho}}) \hat{\mathcal{P}}_{-1,1}^\dagger = \frac{(\gamma_1+\gamma_2)t}{4}(\hat{a}_2^\dagger \hat{a}_1 \bar{\tilde{\rho}} \hat{a}_1^\dagger \hat{a}_2). \tag{C33}$$

We apply the analogous unitary

$$\hat{U}_{-1,1} = |\bar{0}_N\rangle\langle\bar{0}|_{-1,1} + |\bar{1}_N\rangle\langle\bar{1}|_{-1,1}, \tag{C34}$$

which yields

$$\hat{U}_{-1,1}\hat{\mathcal{P}}_{-1,1}\tilde{\mathcal{N}}_D(\bar{\tilde{\rho}})\hat{\mathcal{P}}^\dagger_{-1,1}\hat{U}^\dagger_{-1,1} = \frac{(\gamma_1+\gamma_2)t}{4}(\beta_0^2+\alpha^2 N)\bar{\tilde{\rho}}. \tag{C35}$$

The recovery operation can be written as

$$\tilde{\mathcal{R}}_D \sim \left\{\hat{P}_C\hat{U}_{00}\hat{P}_{00},\ \hat{U}_E^D\hat{P}_E\hat{U}_{00}\hat{P}_{00}, \hat{U}_{1,-1}\hat{P}_{1,-1},\ \hat{U}_{-1,1}\hat{P}_{-1,1}\right\} \cup \{\hat{P}_{lm} \mid \text{all other } (l,m)\}. \tag{C36}$$

Summing Eqs. (C29), (C32), and (C35), its action on the noisy state is therefore

$$\begin{aligned}\tilde{\mathcal{R}}_D \circ \tilde{\mathcal{N}}_D(\bar{\tilde{\rho}}) &= \bar{\tilde{\rho}} + \frac{(\gamma_1+\gamma_2)t}{4}\left(-2\beta_0^2 - 2\alpha^2 N\right) + 2\frac{(\gamma_1+\gamma_2)t}{4}\left(\beta_0^2+\alpha^2 N\right) + \mathcal{O}((\gamma_i t)^2)\\ &= \bar{\tilde{\rho}} + \mathcal{O}((\gamma_i t)^2).\end{aligned} \tag{C37}$$

APPENDIX D: NEAR-OPTIMAL FIDELITY UNDER LOSS AND DEPHASING CHANNELS

In the original work by Michael *et al.* [15], the performance of single-mode binomial codes in the case $N = K$ was investigated for various values of N. For a fixed noise strength κt, they showed that there exists an optimal binomial code with a finite value of N that minimizes the entanglement fidelity among different binomial codes. Motivated by this result, we investigate how this behavior extends to our two-mode binomial codes.

In the two-mode case, the dimension of the codespace grows rapidly with increasing N and K, making it computationally prohibitive to obtain the optimal recovery map via semidefinite programming. To address this challenge, we employ the near-optimal channel fidelity introduced in Ref. [44], which provides an optimization-free metric applicable to arbitrary noise channels and quantum codes. This quantity yields a two-sided bound on the optimal code performance and depends only on the Knill-Laflamme matrix.

The Knill-Laflamme quantum error-correction matrix is defined as

$$M_{[\mu l][\nu k]} = \langle\mu_L|\hat{N}_l^\dagger\hat{N}_k|\nu_L\rangle, \tag{D1}$$

where $|\nu_L\rangle$ are the logical code words and $\{\hat{N}_k\}$ are the Kraus operators of the noise channel $\mathcal{N}$. The near-optimal fidelity is given by

$$\tilde{F}^{\text{opt}} = \frac{1}{d_L^2}\|\text{Tr}_L\sqrt{M}\|_F^2, \tag{D2}$$

where $(\text{Tr}_L B)_{l,k} = \sum_\mu B_{[\mu l],[\mu k]}$, d_L is the logical dimension, and $\|\cdot\|_F$ denotes the Frobenius norm. This quantity provides the following two-sided bound on the optimal fidelity F^{opt}:

$$\tfrac{1}{2}(1-\tilde{F}^{\text{opt}}) \leqslant 1 - F^{\text{opt}} \leqslant 1 - \tilde{F}^{\text{opt}}. \tag{D3}$$

When a code performs well against a given noise channel, the near-optimal fidelity serves as an accurate approximation to the true optimal fidelity. We therefore use these near-optimal bounds to assess the performance of our DRBC for larger values of N and K. The performance under photon loss is shown in Fig. 5(a). For the loss channel, we find that the behavior of the two-mode binomial codes closely mirrors that of the single-mode case. In particular, for small noise strengths, the performance improves with increasing N, while for larger noise strengths there exists an optimal value of N that minimizes the infidelity. This crossover behavior in the single-mode case was previously analyzed in Ref. [15].

However, for purely dephasing channel, as we showed in the previous section that the performance improves for $N \geqslant 4$ as the KL conditions are satisfied up to first order in noise strength, we see a significant improvement unlike the case of the single-mode codes. In Appendix E, we will further show that the KL conditions for continuous representation of dephasing Kraus operators become closer to being satisfied as $N \to \infty$. The numerical results for this analytic proof are given here in Fig. 5. For DBRC with $K = 2$ for optimal encoding angles, we vary N and we plot the optimal fidelity obtained from SDP calculations. We further validate it with results from near-optimal recovery. In this plot, $\mathcal{F}_E$ is the entanglement fidelity that is related to the average gate fidelity as $\mathcal{F} = (2\mathcal{F}_E + 1)/3$ for the qubit encoding.

APPENDIX E: MORE UNDERSTANDING ON PERFORMANCE UNDER DEPHASING FOR TWO-MODE RSB USING PHASE MEASUREMENTS AND KL CONDITIONS OF DUAL CODE WORDS

In Appendix C, we analyzed the effect of the Gaussian dephasing channel using its countable Kraus representation [Eq. (A12)] and constructed a recovery map valid up to first order in the noise strength. We showed that an exact first-order recovery map for the two-mode code can be obtained when the encoding mode is fixed to $\delta = \pi/4$ or $3\pi/4$ (independent of ϕ), provided that the coefficients f_{mn} satisfy the condition given in Eq. (B29).

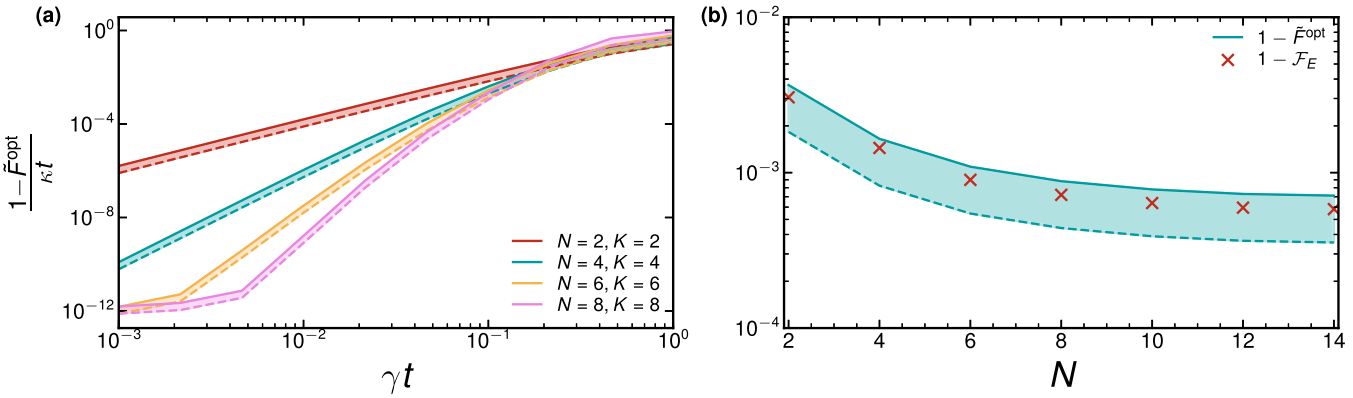

FIG. 5. The solid lines in the figure represent the upper bound of the near-optimal infidelity given by $1 - \tilde{F}^{\text{opt}}$ and the dashed line represents the lower bound given by $\frac{1}{2}(1 - \tilde{F}^{\text{opt}})$. Panel (a) is evaluated for DRBC $N = K$ for only loss as a function of noise strength $\kappa_1 = \kappa_2 = \kappa$. In panel (b), by keeping $K = 2$ and $\gamma_1 t = \gamma_2 t = \gamma t = 0.01$ fixed, we vary N to study the performance with dephasing noise. The infidelity decreases with increase in N, in contrast to the single-mode case.

In this section, we instead consider the Gaussian dephasing channel acting on the two modes in terms of its continuous Kraus representation [13]. Using this representation, we first examine under what conditions the KL criteria are satisfied. We then analyze the distinguishability of the code words under phase measurements in order to gain further insight into the performance of these codes in the presence of dephasing noise.

1. Knill-Laflamme matrix for dual code words under dephasing noise

The effective noisy channel is given by $\tilde{\mathcal{N}} = \hat{U}_{\text{BS}}^{\dagger}\mathcal{N}\hat{U}_{\text{BS}}$, where the noise channel $\mathcal{N}$ can be expanded in terms of the elements of the continuous Kraus operators,

$$\mathcal{N} \sim \{\exp(i\hat{A}(\theta_1, \theta_2)) = e^{i\theta_1\hat{a}_1^{\dagger}\hat{a}_1 + i\theta_2\hat{a}_2^{\dagger}\hat{a}_2} \mid \theta_1, \theta_2 \in [0, 2\pi)\}. \tag{E1}$$

For the effective channel $\tilde{\mathcal{N}}$, the transformed Kraus operators take the form

$$\begin{aligned}\tilde{\hat{A}}(\theta_1, \theta_2) &= \hat{U}_{\text{BS}}^{\dagger}(\theta_1\hat{a}_1^{\dagger}\hat{a}_1 + \theta_2\hat{a}_2^{\dagger}\hat{a}_2)\hat{U}_{\text{BS}} \\ &= \hat{a}_1^{\dagger}\hat{a}_1(\theta_1\cos^2\delta + \theta_2\sin^2\delta) + \hat{a}_2^{\dagger}\hat{a}_2(\theta_2\cos^2\delta + \theta_1\sin^2\delta) \\ &\quad + (\theta_1 - \theta_2)(e^{-i\phi}\hat{a}_1^{\dagger}\hat{a}_2 + e^{i\phi}\hat{a}_2^{\dagger}\hat{a}_1)\sin\delta\cos\delta.\end{aligned} \tag{E2}$$

It is worth noting that the countable Kraus operators for the dephasing channel, $\{(\hat{a}^{\dagger}\hat{a})^l | l \in \mathbb{N}\}$ [13,24], can be expanded in terms of the continuous Kraus operators shown above; the latter are nothing but the rotation operators in the phase space, which allows us to have an intuitive understanding of the *distortion* of information in bosonic systems under dephasing channels. In fact, the dephasing noise can be thought of as diffusion between the probability distributions of the phase measurement outcomes corresponding to the dual code words. If we choose the encoding mode to be given by $\delta = \pi/4$, we obtain

$$\tilde{\hat{A}}(\theta_1, \theta_2) = \tfrac{1}{2}(\hat{a}_1^{\dagger}\hat{a}_1 + \hat{a}_2^{\dagger}\hat{a}_2)(\theta_1 + \theta_2) + \tfrac{1}{2}(\theta_1 - \theta_2)(e^{-i\phi}\hat{a}_1^{\dagger}\hat{a}_2 + e^{i\phi}\hat{a}_2^{\dagger}\hat{a}_1) \tag{E3}$$

$$= \tfrac{1}{2}(\hat{n}_1 + \hat{n}_2)(\theta_1 + \theta_2) + \tfrac{1}{2}(\theta_1 - \theta_2)(\hat{G}_{12}^{+}\cos\phi - \hat{G}_{12}^{-}\sin\phi). \tag{E4}$$

Since $[(\hat{n}_1 + \hat{n}_2), \hat{G}_{12}^{\pm}] = 0$, the noise operator $\exp(i\hat{A}(\theta_1, \theta_2))$ decomposes as

$$\exp\left(\frac{i}{2}(\theta_1 - \theta_2)(\hat{G}_{12}^{+}\cos\phi - \hat{G}_{12}^{-}\sin\phi)\right)\exp\left(\frac{i}{2}(\hat{n}_1 + \hat{n}_2)(\theta_1 + \theta_2)\right). \tag{E5}$$

The off-diagonal entries of the KL matrix in the dual bases for the two error operators with angles (θ_1', θ_2') and (θ_1'', θ_2'') can be now simplified using Eq. (E5) as

$$\langle -_N|\exp(-i\tilde{\hat{A}}(\theta_1', \theta_2'))\exp(i\tilde{\hat{A}}(\theta_1'', \theta_2''))|+_N\rangle = \langle -_N|\exp(i\tilde{\hat{A}}(\theta_1, \theta_2))|+_N\rangle, \tag{E6}$$

where $\theta_i = \theta_i'' - \theta_i'$. Simplifying this further, we obtain

$$\langle -_N|\exp\left(\frac{i}{2}(\theta_1 - \theta_2)(\hat{G}_{12}^{+}\cos\phi - \hat{G}_{12}^{-}\sin\phi)\right)\exp\left(\frac{i}{2}(\hat{n}_1 + \hat{n}_2)(\theta_1 + \theta_2)\right)|+_N\rangle. \tag{E7}$$

We further see that when $\phi = 0$,

$$\begin{aligned}
&\langle -_N| \exp\left(\frac{i}{2}(\theta_1-\theta_2)\hat{G}^+_{12}\right) \exp\left(\frac{i}{2}(\hat{n}_1+\hat{n}_2)(\theta_1+\theta_2)\right)|+_N\rangle \\
&= \langle -_N| e^{-i\frac{\pi}{2}\hat{G}^-_{12}} e^{i\frac{\pi}{2}\hat{G}^-_{12}} \exp\left(\frac{i}{2}(\theta_1-\theta_2)\hat{G}^+_{12}\right) \exp\left(\frac{i}{2}(\hat{n}_1+\hat{n}_2)(\theta_1+\theta_2)\right) e^{-i\frac{\pi}{2}\hat{G}^-_{12}} e^{i\frac{\pi}{2}\hat{G}^-_{12}}|+_N\rangle \\
&= -\langle -_N| e^{i\frac{\pi}{2}\hat{G}^-_{12}} \exp\left(\frac{i}{2}(\theta_1-\theta_2)\hat{G}^+_{12}\right) e^{-i\frac{\pi}{2}\hat{G}^-_{12}} \exp\left(\frac{i}{2}(\hat{n}_1+\hat{n}_2)(\theta_1+\theta_2)\right)|+_N\rangle \\
&= -\langle -_N| e^{-i\pi\hat{n}_2} e^{i\pi\hat{n}_2} \exp\left(-\frac{i}{2}(\theta_1-\theta_2)\hat{G}^+_{12}\right) \exp\left(\frac{i}{2}(\hat{n}_1+\hat{n}_2)(\theta_1+\theta_2)\right) e^{-i\pi\hat{n}_2} e^{i\pi\hat{n}_2}|+_N\rangle \\
&= -\langle -_N| e^{-i\pi\hat{n}_2} e^{i\pi\hat{n}_2} \exp\left(-\frac{i}{2}(\theta_1-\theta_2)\hat{G}^+_{12}\right) \exp\left(\frac{i}{2}(\hat{n}_1+\hat{n}_2)(\theta_1+\theta_2)\right) e^{-i\pi\hat{n}_2} e^{i\pi\hat{n}_2}|+_N\rangle \\
&= -\langle -_N| \exp\left(\frac{i}{2}(\theta_1-\theta_2)\hat{G}^+_{12}\right) \exp\left(\frac{i}{2}(\hat{n}_1+\hat{n}_2)(\theta_1+\theta_2)\right)|+_N\rangle. \qquad \text{(E8)}
\end{aligned}$$

Here, we have used the fact that $e^{i\frac{\pi}{2}\hat{G}^-_{12}}$ acts as the logical X operator on the codespace and N is an even number. We have also used the commutator relation $[\hat{G}^-_{12}, \hat{G}^+_{12}] = 2i(\hat{a}_1^\dagger\hat{a}_1 - \hat{a}_2^\dagger\hat{a}_2)$ from which we also obtain the relation $e^{i\frac{\pi}{2}\hat{G}^-_{12}}\hat{G^+_{12}}e^{-i\frac{\pi}{2}\hat{G}^-_{12}} = -\hat{G^+_{12}}$. Thus, from the above equality in Eq. (E8), we can conclude

$$\langle -_N| \exp\left(\frac{i}{2}(\theta_1-\theta_2)\hat{G}^+_{12}\right) \exp\left(\frac{i}{2}(\hat{n}_1+\hat{n}_2)(\theta_1+\theta_2)\right)|+_N\rangle = 0. \qquad \text{(E9)}$$

For the existence of exact recovery, we further require that the diagonal entries are equal. However, for this channel, we see that they differ as shown below:

$$\begin{aligned}
&\langle +_N| \exp\left(\frac{i}{2}(\theta_1-\theta_2)(\hat{G}^+_{12}\cos\phi - \hat{G}^-_{12}\sin\phi)\right) \exp\left(\frac{i}{2}(\hat{n}_1+\hat{n}_2)(\theta_1+\theta_2)\right)|+_N\rangle \\
&= \langle -_N| e^{-i\frac{\pi}{N}\hat{n}_2} \exp\left(\frac{i}{2}(\theta_1-\theta_2)(\hat{G}^+_{12}\cos\phi - \hat{G}^-_{12}\sin\phi)\right) \exp\left(\frac{i}{2}(\hat{n}_1+\hat{n}_2)(\theta_1+\theta_2)\right) e^{i\frac{\pi}{N}\hat{n}_2}|-_N\rangle \\
&= \langle -_N| \exp\left(\frac{i}{2}(\theta_1-\theta_2)\left(\hat{G}^+_{12}\cos\left(\frac{\pi}{N}-\phi\right) + \hat{G}^-_{12}\sin\left(\frac{\pi}{N}-\phi\right)\right)\right) \exp\left(\frac{i}{2}(\hat{n}_1+\hat{n}_2)(\theta_1+\theta_2)\right)|-_N\rangle, \qquad \text{(E10)}
\end{aligned}$$

where we have used the relations $e^{-i\frac{\pi}{N}\hat{n}_2}\,\hat{G}^\pm_{12}\,e^{i\frac{\pi}{N}\hat{n}_2} = \hat{G}^\pm_{12}\cos\frac{\pi}{N} \pm \hat{G}^\mp_{12}\sin\frac{\pi}{N}$ for the proof. However, from the above expression in Eq. (E10), we see that the two diagonal entries can be brought arbitrarily close to each other by setting $\phi = (2m+1)\frac{\pi}{2N}$ for $m \in \mathbb{Z}$, and taking the limit $N \to \infty$. We also present numerical results in Fig. 5(b) for DRBC to support these findings: As N increases for a fixed K, the average gate infidelity decreases, indicating improved performance. Moreover, we see that for all $\theta_1 = \theta_2$ corresponding to the case of correlated dephasing, the entries given in Eq. (E10) are exactly equal. This justifies the existence of the recovery circuit in Fig. 3. Note that the above discussion holds for any of the general two-mode instantiations of our codes, namely, given by Eqs. (4) and (5).

We exemplify this analytical understanding with numerical calculation of the entanglement infidelity for the case of the DRBC with $N = 2$ and $K = 2$. As shown in Fig. 6, the infidelity is minimized for the optimal encoding angles, $\delta = \pi/4,\ 3\pi/4$ and $\phi = \pi/4$. We have also numerically checked that for $N = 4,\ K = 2$, the infidelity is minimized for the optimal encoding angles, $\delta = \pi/4, 3\pi/4$ and $\phi = \pi/8$ (not shown here).

2. Distinguishing the dual code words and understanding the phase trajectories

In this Appendix, we will see how the two-mode code is distinct in performance under dephasing as compared to a single-mode code in terms of the phase distinguishability of the code words. Similar to the case of single-mode RSB, the dual code words, $|\pm_N\rangle$ encoded in the two-mode RSB, are related by a rotation in either mode, up to a global phase: $\exp(i\frac{\pi}{N}\hat{a}_2^\dagger\hat{a}_2)|\pm_N\rangle = |\mp_N\rangle;\ \exp(i\frac{\pi}{N}\hat{a}_1^\dagger\hat{a}_1)|\pm_N\rangle = -|\mp_N\rangle$.

The *joint phase measurement* in each of the modes formally can be written as a set of POVM: $\{\hat{\Pi}(\phi_1)\otimes\hat{\Pi}(\phi_2) \mid \phi_1, \phi_2 \in [0, 2\pi)\}$, where $\hat{\Pi}(\phi)$ is defined, e.g., in Ref. [30]. The outcomes of such measurement are (ϕ_1, ϕ_2). In the absence of any noise, outcomes $(0, \pi/N) \mod (2\pi/N)$ or $(\pi/N, 0) \mod (2\pi/N)$ indicate that the logical state is $|-_N\rangle$, while the measurement outcomes $(0, 0) \mod (2\pi/N)$ or $(\pi/N, \pi/N) \mod (2\pi/N)$ indicate that the logical state is $|+_N\rangle$ (Fig. 7).

As we have previously found out, for $\delta = 0$ in Eq. (E2), the physical error operators, $\exp(i\hat{A}(0, \pi/N))$ and $\exp(i\hat{A}(\pi/N, 0))$, act as logical Z operator. Hence, the probability distribution of the outcomes of the joint phase measurement can be used to distinguish the code words for *small enough* rotation errors only, parametrized by $\theta_1, \theta_2 \ll \pi/N$. This allows us to distinguish the

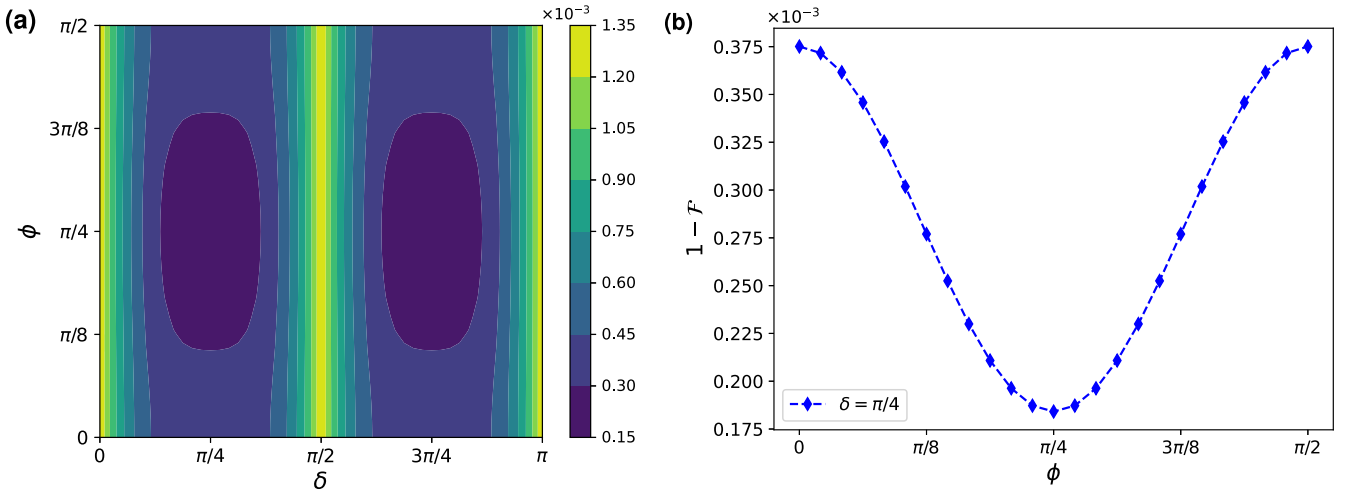

FIG. 6. (a) Entanglement infidelity as a function of δ and ϕ, showing minima for $\delta = \pi/4, 3\pi/4$ for $N = 2$, $K = 2$ DRBC against dephasing $\gamma_1 t = \gamma_2 t = 10^{-3}$. (b) The variation of entanglement infidelity as a function of ϕ is very small (of the order 10^{-3}). We, however, still observe that the lowest value is obtained from $\phi = \pi/4$, which is $\pi/(2N)$ for $N = 2$ and $m = 0$.

dual code words with high accuracy for small enough errors. However, for large rotation errors, for example, $(\pi/N, 0)$, $(0, \pi/N)$, the joint probability distribution for the dual code words maps into one another, as these errors act as logical Z operator.

On the other hand, if we consider the case, $\delta = \pi/4$, from Eq. (E2) we have

$$\tilde{\hat{A}}(\theta_1, \theta_2) = \tfrac{1}{2}(\hat{a}_1^\dagger \hat{a}_1 + \hat{a}_2^\dagger \hat{a}_2)(\theta_1 + \theta_2) + \tfrac{1}{2}(\theta_1 - \theta_2)(e^{-i\phi}\hat{a}_1^\dagger \hat{a}_2 + e^{i\phi}\hat{a}_2^\dagger \hat{a}_1) \tag{E11}$$

$$= \tfrac{1}{2}(\hat{n}_1 + \hat{n}_2)(\theta_1 + \theta_2) + \tfrac{1}{2}(\theta_1 - \theta_2)(\hat{G}_+ \cos\phi - \hat{G}_- \sin\phi). \tag{E12}$$

As we know that $[(\hat{n}_1 + \hat{n}_2), \hat{G}_\pm] = 0$, the noise operators decomposes as

$$\tilde{\hat{A}}(\theta_1, \theta_2) = \exp\left(\frac{i}{2}(\theta_1 - \theta_2)(\hat{G}_+ \cos\phi - \hat{G}_- \sin\phi)\right) \exp\left(\frac{i}{2}(\hat{n}_1 + \hat{n}_2)(\theta_1 + \theta_2)\right). \tag{E13}$$

As shown in Appendix E, and in particular in Eq. (E9), for $\delta = \pi/4$ and $\phi = 0$, the overlap between the code words as it evolves under the dephasing Kraus operators remains zero:

$$\langle -_N | \exp(i\tilde{\hat{A}}(\theta_1, \theta_2)) | +_N \rangle = 0 \quad \forall \theta_1, \theta_2. \tag{E14}$$

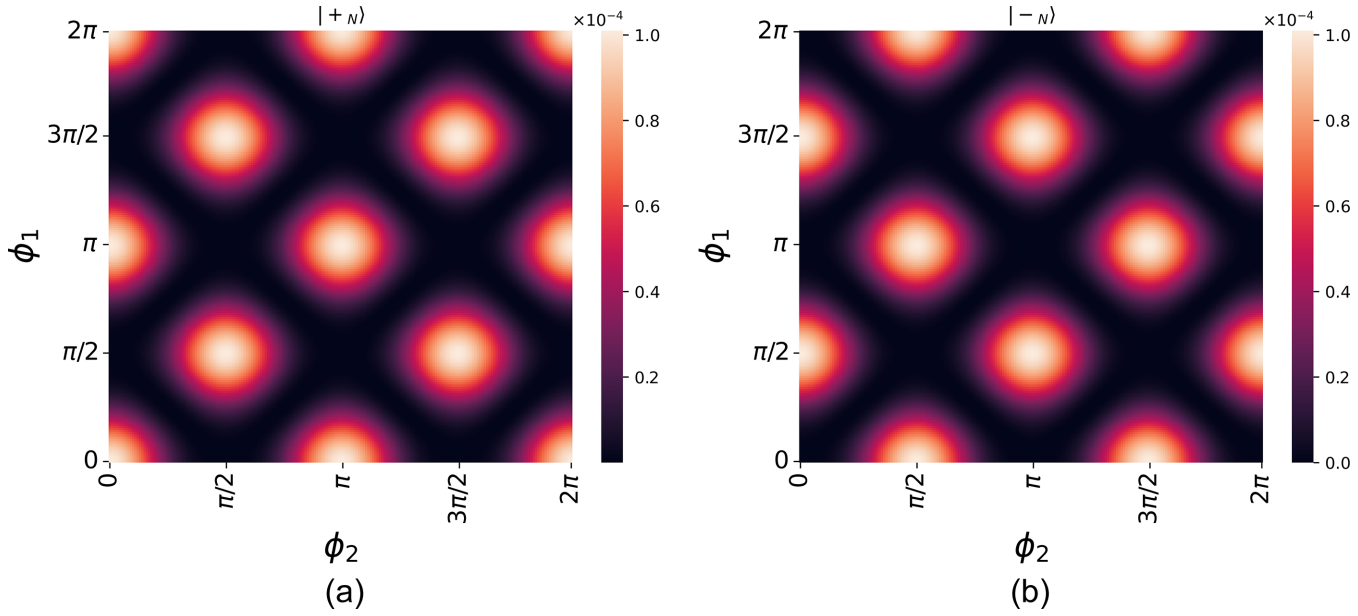

FIG. 7. Probability distribution of phase measurement outcome for the dual basis encoded in $K = 2, N = 2$ two-mode code.

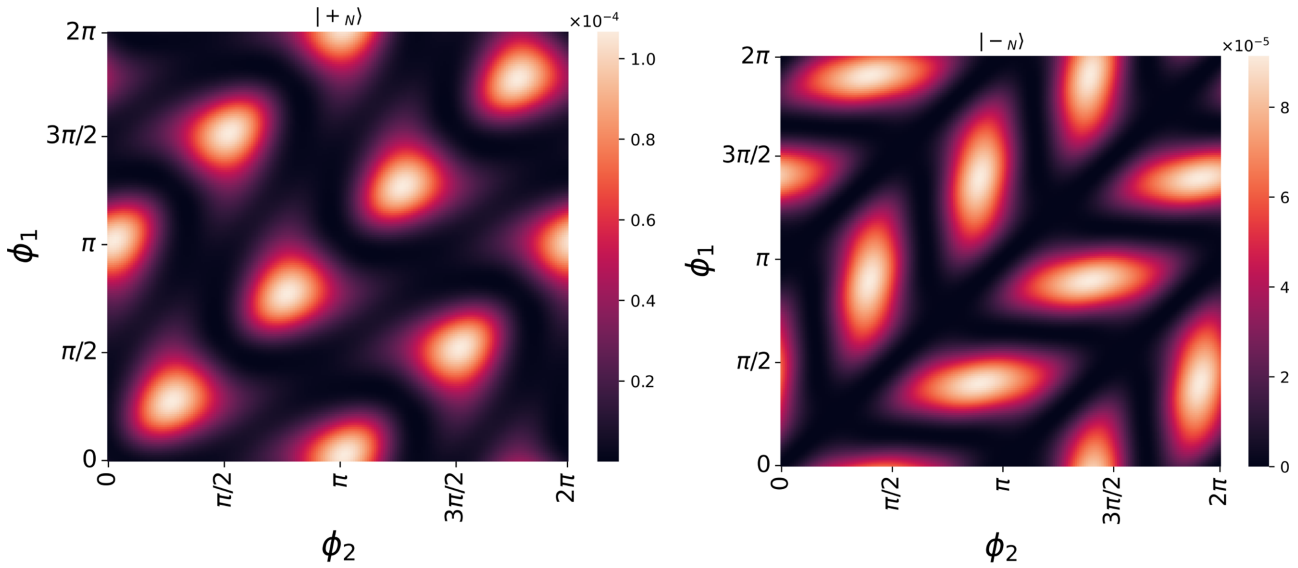

FIG. 8. Probability distribution of phase measurement outcome for the dual basis encoded in $K = 2$, $N = 2$ two-mode code under a rotation $\exp(i\hat{A}(0.2\pi, 0))$ for the encoding axis given by $\delta = \frac{\pi}{4}$, $\phi = 0$.

This is in stark contrast with the single-mode and $\delta = 0$ two-mode cases, where the overlap can be nonzero. Moreover, if we look at the joint probability distribution of phase measurement outcomes of the dual code words as shown in Fig. 8, we find that their support is largely mutually exclusive for all rotation errors. This allows us to distinguish the dual code words with high accuracy, even for large rotation errors. However, we reemphasize that exact error correction is generally still not possible since as shown in the previous Appendix, the diagonal entries of the Knill-Laflamme equations are not equal [Eq. (E10)].

It should also be noted that Eq. (E14) holds true for Gaussian dephasing alone, and does not imply that the evolution of trace distance between the code words under an arbitrary dephasing channel is always unity. In general, the noisy code words are not perfectly distinguishable for an arbitrary dephasing channel. A future work may explore whether such nonoverlapping distribution of the outcomes of phase measurements can be used to design an error-correcting circuit similar to the teleportation circuit due to Knill [13,45]. Finally, also note that for DRBC, as the energy of the binomial codes (parametrized by K for binomial codes) increases, the probability distribution of the outcomes for the dual code words has vanishing overlap [13], suggesting a better performance against the dephasing noise can be found with increasing K (while with losses a sweet spot in average energy is to be expected).

APPENDIX F: PERFORMANCE OF TWO-MODE ROTATION-SYMMETRIC BOSONIC CODES UNDER THE INFLUENCE OF RANDOM TELEGRAPH NOISE

Here, we present numerical results on the performance of simple instances of our DRBC ($K = 2,\ N = 2$), for different choices of the encoding angles, against random telegraph noise. ξ is the switching rate and ν is the amplitude of the RTN. We refer to Ref. [30] for a thorough definition of the noise, along with the parameters. The plot in Fig. 9 shows that the optimal encoding angles yield an increased performance against RTN noise, and that such performance beats the case of the corresponding single-mode binomial code.

APPENDIX G: EXACT RECOVERY CIRCUIT FOR CORRELATED DEPHASING

Here, we show that correlated dephasing can be corrected perfectly, and we derive the corresponding recovery map. Since the beam-splitting operation $\hat{U}_{\rm BS}$ commutes with the Kraus operators of correlated dephasing, i.e., $[(\hat{n}_1 + \hat{n}_2), U_{\rm BS}(\delta, \phi)] = 0$ for each δ, ϕ, the analysis holds independently of the choice of encoding angles.

First, we wish to study the action of the controlled operation

$$\mathrm{CX}_{NL} = \exp\left(i\frac{\pi}{2N}\hat{n}_1 \otimes \hat{G}^{-}_{34}\right)$$

on the four-mode Fock states appearing in the tensor product of two code words provided in the main text, which we report here for convenience.

To do so, we first look explicitly at the action of beam-splitter operations of the type in Eq. (A7) on states of the form $|rN, sN\rangle$, with r and s two integer numbers. The operator $e^{i\delta\hat{G}^{-}_{12}}$ corresponds to setting the angle $\phi = 2\pi k$ with k integer in Eq. (A7). Its

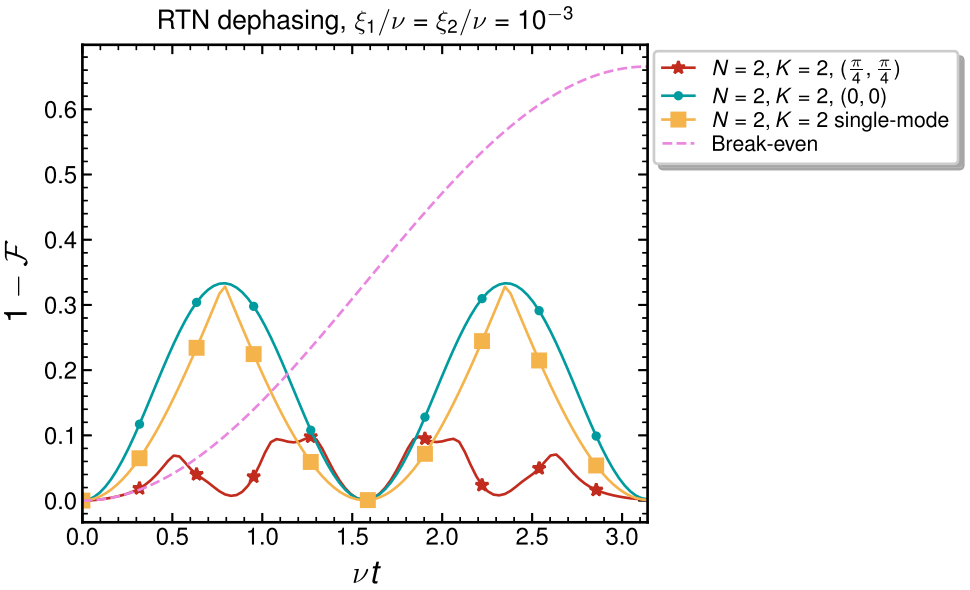

FIG. 9. A comparison between the optimal performance of the single-mode binomial code, $K = 2,\ N = 2$ and the simplest instance of the two-mode order-N RSB code, $K = 2,\ N = 2$ inner binomial concatenated with outer dual rail. Specifically, we investigate the performance of the code, upon a beam-splitting action with angle $(\pi/4,\ \pi/4)$ after the preparation of the logical state in the modes $\hat{a}_1, \hat{a}_2$.

action can be expressed as

$$\begin{aligned} e^{i\delta\hat{G}_{12}^{-}}|rN, sN\rangle &= \left(e^{i\delta\hat{G}_{12}^{-}}\frac{(\hat{a}_1^\dagger)^{rN}}{\sqrt{(rN)!}}e^{-i\delta\hat{G}_{12}^{-}}\right)\left(e^{i\delta\hat{G}_{12}^{-}}\frac{(\hat{a}_2^\dagger)^{sN}}{\sqrt{(sN)!}}e^{-i\delta\hat{G}_{12}^{-}}\right)|0,0\rangle \\ &= \frac{(\hat{a}_1^\dagger\cos\delta + \hat{a}_2^\dagger\sin\delta)^{rN}}{\sqrt{(rN)!}}\frac{(\hat{a}_2^\dagger\cos\delta - \hat{a}_1^\dagger\sin\delta)^{sN}}{\sqrt{(sN)!}}|0,0\rangle, \end{aligned} \tag{G1}$$

where we have used Eq. (A8) for $\phi = 2\pi k$, and the fact that the operator $e^{i\delta\hat{G}_{12}^{-}}$ acts as the identity on the two-mode vacuum.

The previous equation reduces for some values of δ to the two relevant cases:

$$\begin{aligned} &\text{for } \delta = \pi m \to e^{i\delta\hat{G}_{12}^{-}}|rN, sN\rangle = (-1)^{mN(r+s)}\frac{(\hat{a}_1^\dagger)^{rN}}{\sqrt{(rN)!}}\frac{(\hat{a}_2^\dagger)^{sN}}{\sqrt{(sN)!}}|0,0\rangle = |rN, sN\rangle, \\ &\text{for } \delta = (2n+1)\frac{\pi}{2} \to e^{i\delta\hat{G}_{12}^{-}}|rN, sN\rangle = (-1)^{nN(r-s)}\frac{(\hat{a}_1^\dagger)^{rN}}{\sqrt{(rN)!}}\frac{(\hat{a}_2^\dagger)^{sN}}{\sqrt{(sN)!}}|0,0\rangle = |rN, sN\rangle, \end{aligned} \tag{G2}$$

where we have used that N is even. As a consequence of this, the action of the controlled operation on the four-mode Fock states appearing in the tensor product of two code words of the form in Eqs. (4) and (5) gives

$$\begin{aligned} \text{CX}_{NL}|2mN, (2n+1)N\rangle \otimes |2pL, (2q+1)L\rangle &= |2mN, (2n+1)N\rangle \otimes e^{i\pi m\hat{G}_{34}^{-}}|2pL, (2q+1)L\rangle \\ &= |2mN, (2n+1)N\rangle|2pL, (2q+1)L\rangle, \end{aligned} \tag{G3}$$

$$\begin{aligned} \text{CX}_{NL}|2mN, (2n+1)N\rangle \otimes |(2q+1)L, 2pL\rangle &= |2mN, (2n+1)N\rangle \otimes e^{i\pi m\hat{G}_{34}^{-}}|(2q+1)L, 2pL\rangle \\ &= |2mN, (2n+1)N\rangle|(2q+1)L, 2pL\rangle, \end{aligned} \tag{G4}$$

$$\begin{aligned} \text{CX}_{NL}|(2n+1)N, 2mN\rangle \otimes |2pL, (2q+1)L\rangle &= |(2n+1)N, 2mN\rangle \otimes e^{i\frac{\pi}{2}(2n+1)\hat{G}_{34}^{-}}|2pL, (2q+1)L\rangle \\ &= |(2n+1)N, 2mN\rangle \otimes |(2q+1)L, 2pL\rangle, \end{aligned} \tag{G5}$$

$$\begin{aligned} \text{CX}_{NL}|(2n+1)N, 2mN\rangle \otimes |(2q+1)L, 2pL\rangle &= |(2n+1)N, 2mN\rangle \otimes e^{i\frac{\pi}{2}(2n+1)\hat{G}_{34}^{-}}|(2q+1)L, 2pL\rangle \\ &= |(2n+1)N, 2mN\rangle \otimes |2pL, (2q+1)L\rangle. \end{aligned} \tag{G6}$$

Summing the terms in Eq. (G3) over the indices $m,\ n,\ p,$ and q in the above expressions, one finds that $\text{CX}_{NL}|0\rangle_N \otimes |a\rangle_L = |0\rangle_N \otimes |a\rangle_L$ and $\text{CX}_{NL}|1\rangle_N \otimes |a\rangle_L = |1\rangle_N \otimes |a \oplus a\rangle_L$, indicating that it acts as a controlled-X gate on the codespace of the two-mode codes.

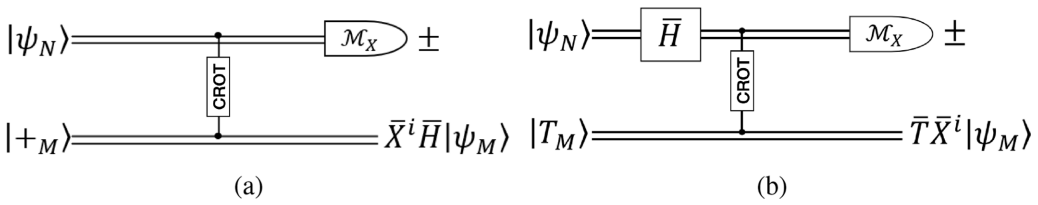

FIG. 10. Implementation of (a) the Hadamard gate and (b) T gate for the two-mode rotation-symmetric codes using gate teleportation.

Using these expressions, the map corresponding to the circuit in Fig. 3, with $\mathrm{CX}_{LN} = \exp(i\frac{\pi}{2N}\hat{n}_3 \otimes \hat{G}^-_{21})$, is given by

$$\begin{aligned}\mathcal{R}(\mathcal{N}(\hat{\rho})\otimes|0\rangle\langle 0|_L) &= \mathrm{CX}_{LN}\mathrm{CX}_{NL}(\mathcal{N}(\hat{\rho})\otimes|0\rangle\langle 0|_L)\mathrm{CX}^\dagger_{NL}\mathrm{CX}^\dagger_{LN}\\ &= \sum_{a,b=0,1}\rho_{ab}\mathrm{CX}_{LN}\mathrm{CX}_{NL}\left(\int_{-\infty}^{\infty}\mathrm{d}\phi\ p_t(\phi)e^{i\phi(\hat{n}_1+\hat{n}_2)}\ |a\rangle\langle b|_N\ e^{-i\phi(\hat{n}_1+\hat{n}_2)}\otimes|0\rangle\langle 0|_L\right)\mathrm{CX}^\dagger_{NL}\mathrm{CX}^\dagger_{LN}\\ &= \sum_{a,b=0,1}\rho_{ab}\left(\int_{-\infty}^{\infty}\mathrm{d}\phi\ p_t(\phi)e^{i\phi(\hat{n}_1+\hat{n}_2)}\ \mathrm{CX}_{LN}|a\rangle\langle b|_N\otimes|a\rangle\langle b|_L\mathrm{CX}^\dagger_{LN}\ e^{-i\phi(\hat{n}_1+\hat{n}_2)}\right).\end{aligned} \tag{G7}$$

Here, we have used the fact that the CX gate commutes with the correlated dephasing operator, since $[(\hat{n}_i+\hat{n}_j),\hat{G}^-_{ij}]=0$, and that the controlled-X operation satisfies $\mathrm{CX}_{NL}|a\rangle_N|0\rangle_L = |a\rangle_N|a\rangle_L$.

For a given a and b, we further find that

$$\begin{aligned}\mathrm{CX}_{LN}|a\rangle_N\otimes|a\rangle_L\langle b|_N\otimes\langle b|_L\mathrm{CX}^\dagger_{LN} &= |(a\oplus a)\rangle_N\otimes|a\rangle_L\langle(b\oplus b)|_N\otimes\langle b|_L\\ &= |0\rangle\langle 0|_N\otimes|a\rangle\langle b|_L.\end{aligned} \tag{G8}$$

Substituting this into Eq. (G7), we obtain

$$\begin{aligned}\mathcal{R}(\mathcal{N}(\hat{\rho})\otimes|0\rangle\langle 0|_L) &= \left(\int_{-\infty}^{\infty}\mathrm{d}\phi\ p_t(\vec{\phi})e^{i\phi(\hat{n}_1+\hat{n}_2)}\ |0\rangle\langle 0|_N\ e^{-i\phi(\hat{n}_1+\hat{n}_2)}\right)\otimes\sum_{a,b=0,1}\rho_{ab}|a\rangle\langle b|_L\\ &= \mathcal{N}(|0\rangle\langle 0|_N)\otimes\sum_{a,b=0,1}\rho_{ab}|a\rangle\langle b|_L.\end{aligned} \tag{G9}$$

This holds for an arbitrary choice of the two-mode code words in Eqs. (4) and (5), not only for the case of binomial codes.

APPENDIX H: HADAMARD GATE AND T GATE

In this section, we include the circuits that implement the Hadamard and T gates via gate teleportation. The schemes are direct extensions of those proposed for single-mode RSB codes [13] to the two-mode setting (see Fig. 10). We first show how the controlled rotation (CROT) gate acts as a logical controlled-Z (CZ) gate on our encoded two-mode codespace.

The CROT gate is defined as

$$\mathrm{CROT}_{NL} = \exp\left(\frac{i\pi}{NL}\hat{n}_1\otimes\hat{n}_3\right),$$

where $\hat{n}_1$ and $\hat{n}_3$ are the photon number operators associated with the first modes of the control and target rails, respectively. The gate acts on the four-mode Fock states appearing in the tensor product of two code words as

$$\begin{aligned}\mathrm{CROT}_{NL}|2mN,(2n+1)N\rangle\otimes|2pL,(2q+1)L\rangle &= e^{i\pi 2m2p}|2mN,(2n+1)N\rangle\otimes|2pL,(2q+1)L\rangle\\ &= |2mN,(2n+1)N\rangle|2pL,(2q+1)L\rangle,\end{aligned} \tag{H1}$$

$$\begin{aligned}\mathrm{CROT}_{NL}|2mN,(2n+1)N\rangle\otimes|(2q+1)L,2pL\rangle &= e^{i\pi 2m(2q+1)}|2mN,(2n+1)N\rangle\otimes|(2q+1)L,2pL\rangle\\ &= |2mN,(2n+1)N\rangle|(2q+1)L,2pL\rangle,\end{aligned} \tag{H2}$$

$$\begin{aligned}\mathrm{CROT}_{NL}|(2n+1)N,2mN\rangle\otimes|2pL,(2q+1)L\rangle &= e^{i\pi(2n+1)2p}|(2n+1)N,2mN\rangle\otimes|2pL,(2q+1)L\rangle\\ &= |(2n+1)N,2mN\rangle\otimes|2pL,(2q+1)L\rangle,\end{aligned} \tag{H3}$$

$$\begin{aligned}\mathrm{CROT}_{NL}|(2n+1)N,2mN\rangle\otimes|(2q+1)L,2pL\rangle &= e^{i\pi(2n+1)(2q+1)}|(2n+1)N,2mN\rangle\otimes|(2q+1)L,2pL\rangle\\ &= -|(2n+1)N,2mN\rangle\otimes|(2q+1)L,2pL\rangle.\end{aligned} \tag{H4}$$

Summing over the indices, one can verify that CROT_{NL} acts as a controlled-Z gate on the logical codespace $\{|a_N\rangle \otimes |b_L\rangle,\ a, b \in \{0, 1\}\}$.

To illustrate the Hadamard-gate protocol in Fig. 10(a), we first prepare an auxiliary two-mode encoded qubit in the state $|+_M\rangle = \frac{1}{\sqrt{2}}(|0_M\rangle + |1_M\rangle)$ and entangle it with the state $|\psi_N\rangle = \alpha|0_N\rangle + \beta|1_N\rangle$ to be teleported:

$$\text{CROT}|\psi_N\rangle \otimes |+_M\rangle = \alpha|0_N\rangle|+_M\rangle + \beta|1_N\rangle|-_M\rangle. \tag{H5}$$

Rewriting the order-N state in the $\pm$ basis and the order-M state in the computational basis, we obtain

$$\text{CROT}|\psi_N\rangle \otimes |+_M\rangle = \frac{\alpha}{2}(|+_N\rangle + |-_N\rangle) \otimes (|0_M\rangle + |1_M\rangle) + \frac{\beta}{2}(|+_N\rangle - |-_N\rangle) \otimes (|0_M\rangle - |1_M\rangle). \tag{H6}$$

Measuring the first (control) rail in the $\pm$ basis yields the output state on the target rail as $\alpha|+_M\rangle + \beta|-_M\rangle$ for the outcome "+" and $\alpha|+_M\rangle - \beta|-_M\rangle$ for the outcome "−". Combining both cases, with $i = 0$ for "+" and $i = 1$ for "−", the output state is

$$\bar{X}^i \bar{H}|\psi_M\rangle, \tag{H7}$$

where $\bar{H}$ acts as the logical Hadamard gate on the two-mode codespace.

The same reasoning applies for the T-gate circuit in Fig. 10(b). Writing $|T_M\rangle = \frac{1}{\sqrt{2}}(|0_M\rangle + e^{\frac{i\pi}{4}}|1_M\rangle)$, one obtains the logical $\bar{T}$ or $\bar{T}\bar{X}$ gate depending on whether the measurement outcome is "+" or "−", respectively.

[1] V. V. Albert, Bosonic coding: Introduction and use cases, in *Quantum Fluids of Light and Matter*, edited by A. Bramati, I. Carusotto, and C. Ciuti (IOS Press, Amsterdam, 2025), pp. 79–107.

[2] Z. Ni, S. Li, X. Deng, Y. Cai, L. Zhang, W. Wang, Z.-B. Yang, H. Yu, F. Yan, S. Liu, *et al.*, Beating the break-even point with a discrete-variable-encoded logical qubit, Nature (London) **616**, 56 (2023).

[3] V. Sivak, A. Eickbusch, B. Royer, S. Singh, I. Tsioutsios, S. Ganjam, A. Miano, B. Brock, A. Ding, L. Frunzio, *et al.*, Real-time quantum error correction beyond break-even, Nature (London) **616**, 50 (2023).

[4] D. K. Tuckett, S. D. Bartlett, and S. T. Flammia, Ultrahigh error threshold for surface codes with biased noise, Phys. Rev. Lett. **120**, 050505 (2018).

[5] J. Zhang, Y.-C. Wu, and G.-P. Guo, Concatenation of the Gottesman-Kitaev-Preskill code with the XZZX surface code, Phys. Rev. A **107**, 062408 (2023).

[6] K. Noh and C. Chamberland, Fault-tolerant bosonic quantum error correction with the surface–Gottesman-Kitaev-Preskill code, Phys. Rev. A **101**, 012316 (2020).

[7] K. Noh, C. Chamberland, and F. G. S. L. Brandão, Low-overhead fault-tolerant quantum error correction with the surface-GKP code, PRX Quantum **3**, 010315 (2022).

[8] K. Fukui, A. Tomita, A. Okamoto, and K. Fujii, High-threshold fault-tolerant quantum computation with analog quantum error correction, Phys. Rev. X **8**, 021054 (2018).

[9] N. Raveendran, N. Rengaswamy, F. Rozpędek, A. Raina, L. Jiang, and B. Vasić, Finite rate QLDPC-GKP coding scheme that surpasses the CSS Hamming bound, Quantum **6**, 767 (2022).

[10] L. Berent, T. Hillmann, J. Eisert, R. Wille, and J. Roffe, Analog information decoding of bosonic quantum low-density parity-check codes, PRX Quantum **5**, 020349 (2024).

[11] D. Ruiz, J. Guillaud, A. Leverrier, M. Mirrahimi, and C. Vuillot, LDPC-cat codes for low-overhead quantum computing in 2D, Nat. Commun. **16**, 1040 (2025).

[12] É. Gouzien, D. Ruiz, F.-M. Le Régent, J. Guillaud, and N. Sangouard, Performance analysis of a repetition cat code architecture: Computing 256-bit elliptic curve logarithm in 9 hours with 126 133 cat qubits, Phys. Rev. Lett. **131**, 040602 (2023).

[13] A. L. Grimsmo, J. Combes, and B. Q. Baragiola, Quantum computing with rotation-symmetric bosonic codes, Phys. Rev. X **10**, 011058 (2020).

[14] A. Denys and A. Leverrier, Quantum error-correcting codes with a covariant encoding, Phys. Rev. Lett. **133**, 240603 (2024).

[15] M. H. Michael, M. Silveri, R. T. Brierley, V. V. Albert, J. Salmilehto, L. Jiang, and S. M. Girvin, New class of quantum error-correcting codes for a bosonic mode, Phys. Rev. X **6**, 031006 (2016).

[16] Even though the physical representation is given using the passive linear operations on the d modes, note its difference from the one given in Ref. [14], which assumes a physical representation that is isomorphic to the Pauli group itself while the one proposed here is more general.

[17] M. Bergmann and P. van Loock, Quantum error correction against photon loss using NOON states, Phys. Rev. A **94**, 012311 (2016).

[18] L. García-Álvarez, C. Calcluth, A. Ferraro, and G. Ferrini, Efficient simulatability of continuous-variable circuits with large Wigner negativity, Phys. Rev. Res. **2**, 043322 (2020).

[19] Y. Xu, Y. Wang, and V. V. Albert, Multimode rotation-symmetric bosonic codes from homological rotor codes, Phys. Rev. A **110**, 022402 (2024).

[20] E. Descamps, A. Keller, and P. Milman, Gottesman-Kitaev-Preskill encoding in continuous modal variables of single photons, Phys. Rev. Lett. **132**, 170601 (2024).

[21] We further note that for the code words defined in Eqs. (4) and (5), when N is odd, the implementation of the Z gate remains unchanged and the logical X gate can instead be implemented as $\hat{U}_{\text{BS}} e^{-i\pi \hat{G}_{\overline{12}}/2} e^{i\pi \hat{a}_1^\dagger \hat{a}_1/N} \hat{U}_{\text{BS}}^\dagger$.

[22] E. Knill, R. Laflamme, and G. J. Milburn, A scheme for efficient quantum computation with linear optics, Nature (London) **409**, 46 (2001).

[23] J. Guillaud and M. Mirrahimi, Repetition cat qubits for fault-tolerant quantum computation, Phys. Rev. X **9**, 041053 (2019).

[24] V. V. Albert, S. O. Mundhada, A. Grimm, S. Touzard, M. H. Devoret, and L. Jiang, Pair-cat codes: Autonomous error-correction with low-order nonlinearity, Quantum Sci. Technol. **4**, 035007 (2019).

[25] S. S. Chelluri, S. Sharma, F. Schmidt, S. V. Kusminskiy, and P. van Loock, Bosonic quantum error correction with microwave cavities for quantum repeaters, arXiv:2503.21569.

[26] J. Steinbach and J. Twamley, Motional quantum error correction, J. Mod. Opt. **47**, 453 (2000).

[27] Furthermore, our codes are also distinct from the bosonic quantum Fourier codes based on cat states along a similar group-theoretic construction [43].

[28] I. L. Chuang, D. W. Leung, and Y. Yamamoto, Bosonic quantum codes for amplitude damping, Phys. Rev. A **56**, 1114 (1997).

[29] A. S. Fletcher, P. W. Shor, and M. Z. Win, Optimum quantum error recovery using semidefinite programming, Phys. Rev. A **75**, 012338 (2007).

[30] A. Udupa, T. Hillmann, R. G. Ahmed, A. Smirne, and G. Ferrini, Performance of rotation-symmetric bosonic codes in the presence of non-Markovian effects induced by random telegraph noise, Phys. Rev. Res. **8**, 023007 (2026).

[31] U. Leonhardt, J. A. Vaccaro, B. Böhmer, and H. Paul, Canonical and measured phase distributions, Phys. Rev. A **51**, 84 (1995).

[32] J. Bergli, Y. M. Galperin, and B. L. Altshuler, Decoherence of a qubit by non-Gaussian noise at an arbitrary working point, Phys. Rev. B **74**, 024509 (2006).

[33] J. Bergli, Y. M. Galperin, and B. L. Altshuler, Decoherence in qubits due to low-frequency noise, New J. Phys. **11**, 025002 (2009).

[34] J. Schriefl, Y. Makhlin, A. Shnirman, and G. Schön, Decoherence from ensembles of two-level fluctuators, New J. Phys. **8**, 1 (2006).

[35] C. Müller, J. H. Cole, and J. Lisenfeld, Towards understanding two-level-systems in amorphous solids: Insights from quantum circuits, Rep. Prog. Phys. **82**, 124501 (2019).

[36] C. Benedetti, M. G. A. Paris, and S. Maniscalco, Non-Markovianity of colored noisy channels, Phys. Rev. A **89**, 012114 (2014).

[37] R. Lescanne, M. Villiers, T. Peronnin, A. Sarlette, M. Delbecq, B. Huard, T. Kontos, M. Mirrahimi, and Z. Leghtas, Exponential suppression of bit-flips in a qubit encoded in an oscillator, Nat. Phys. **16**, 509 (2020).

[38] B. J. Chapman, S. J. de Graaf, S. H. Xue, Y. Zhang, J. Teoh, J. C. Curtis, T. Tsunoda, A. Eickbusch, A. P. Read, A. Koottandavida, S. O. Mundhada, L. Frunzio, M. H. Devoret, S. M. Girvin, and R. J. Schoelkopf, High-on-off-ratio beamsplitter interaction for gates on bosonically encoded qubits, PRX Quantum **4**, 020355 (2023).

[39] B. Royer, S. Singh, and S. M. Girvin, Encoding qubits in multimode grid states, PRX Quantum **3**, 010335 (2022).

[40] Nord Quantique, Suppressing logical errors with multimode quantum error correction, (2025), https://nordquantique.com/articles/suppressing-logical-errors-multimode-quantum-error-correction/.

[41] T. Hillmann, F. Quijandría, G. Johansson, A. Ferraro, S. Gasparinetti, and G. Ferrini, Universal gate set for continuous-variable quantum computation with microwave circuits, Phys. Rev. Lett. **125**, 160501 (2020).

[42] A. M. Eriksson, T. Sépulcre, M. Kervinen, T. Hillmann, M. Kudra, S. Dupouy, Y. Lu, M. Khanahmadi, J. Yang, C. Castillo-Moreno, *et al.*, Universal control of a bosonic mode via drive-activated native cubic interactions, Nat. Commun. **15**, 2512 (2024).

[43] A. Leverrier, Bosonic quantum Fourier codes, Quantum **10**, 2000 (2026).

[44] G. Zheng, W. He, G. Lee, and L. Jiang, Near-optimal performance of quantum error correction codes, Phys. Rev. Lett. **132**, 250602 (2024).

[45] T. Hillmann, F. Quijandría, A. L. Grimsmo, and G. Ferrini, Performance of teleportation-based error-correction circuits for bosonic codes with noisy measurements, PRX Quantum **3**, 020334 (2022).